CHAPTER II

REVIEW OF RELATED LITERATURE AND RESEARCH

Knowledge diagram

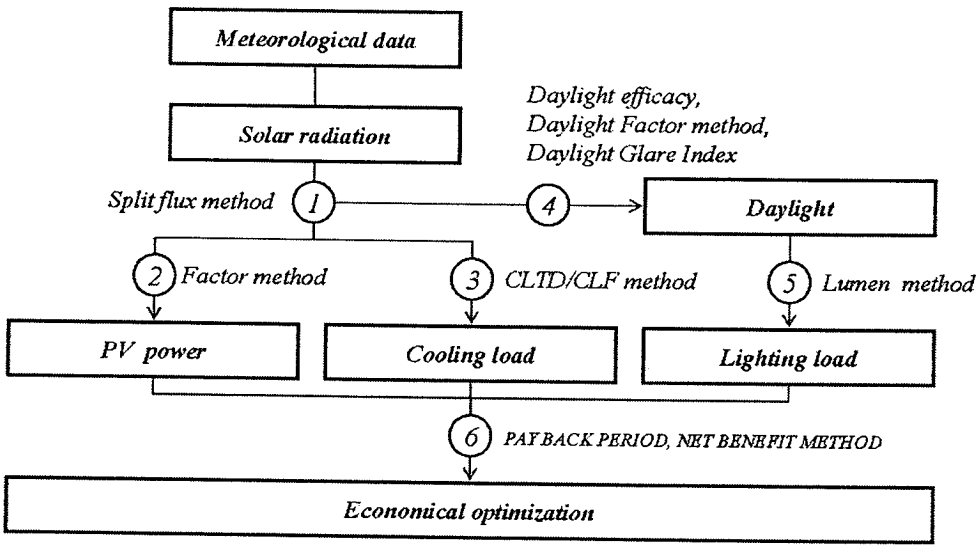

Figure 17 Diagram of knowledge for studing

Meteorological data

This study is related to solar energy and the climate of Thailand which has characteristics different from cold countries. Studying an actual database collected from area of interest was practiced to anticipate the values. The results were more accurate than using the default data of the equation value anticipation program. Metrological data for this research consists of global solar radiation, diffuse solar radiation and ambient temperature collected by the Thai Meteorological Department (TMD) and from the School of Renewable Energy Technology (SERT), where data is managed hourly for the whole year in the form of a typical meteorological year (TMY).

However, collected data is different every year depending on influences of phenomena such as monsoon, cold and warm current, etc. The data study was studied over 5 years in 2006-2010 as presented in Table 2.

Table 2 The weather data during the year

Year	Condition compare with normal year (average of 1971-2000)
2006	7% over for raining, almost hotter, 2 tropical cyclone
2007	4% over for raining, almost hotter, 3 tropical cyclone
2008	11% over for raining, almost hotter, 1 tropical cyclone and 3 closer
2009	4% over for raining, almost hotter, 1 tropical cyclone
2010	5% over for raining, all hotter, 1 tropical cyclone

Source: Thai Meteorological Department [86, 87, 88, 89, 90]

Solar radiation

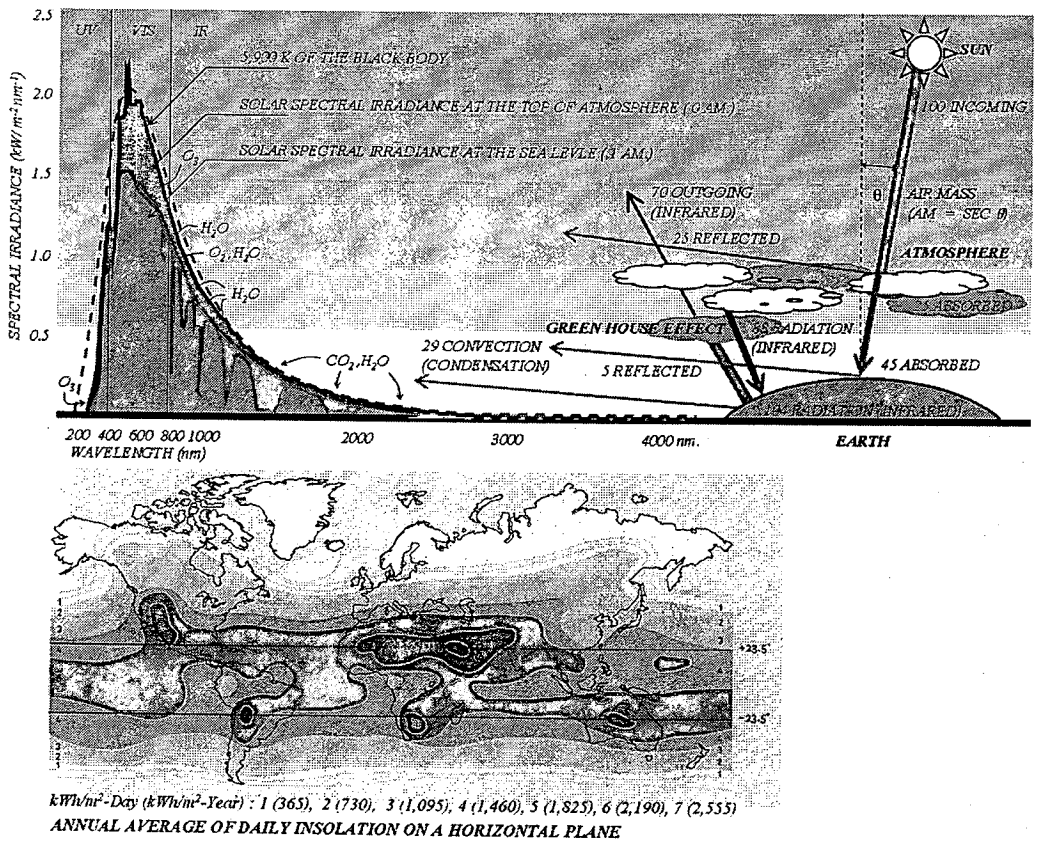

Figure 18 Solar insolation on earth

Source: Simon Roberts and Nicolo Guariento [27]; Learner, Annenberg [73]

The solar radiation, electromagnetic radiation passing through the earth's atmosphere down to the surface, about 45% is absorbed and 30% is reflected back. However, 25% is absorbed by atmosphere composed of ozone, carbon dioxide and water vapor.

In studying solar radiation, sun-earth angle was used for this research to estimate total irradiance on slope surface in both cases of a PV module and a glass window. As Thailand is located in a tropical zone with a large amount of vapor and dust in the air, variables regarding location and weather such as latitude, longitude, weather data and solar radiation should be considered in estimation of any values. Therefore, specific characteristics of design conditions will be revealed, as shown in Figure 19 explaining the process in solar irradiance calculation.

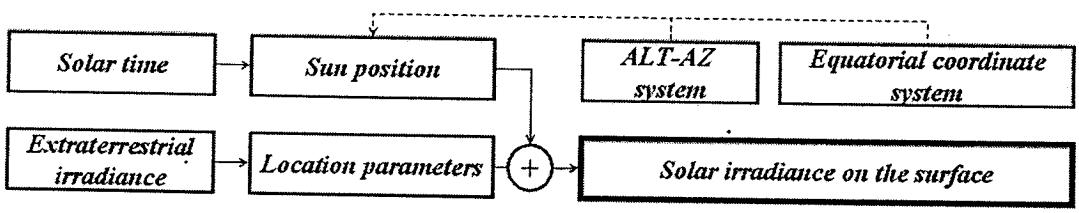

Figure 19 The calculation's process of solar irradiance on the surface

1. Solar time

Figure 20 shows the relation of earth-sun position, which is the system of positioning changed by the time of day. Solar time is calculated by the equation [19] as follows:

$$t_S = t_{SL} + (EOT / 60) + [(L_{SM} - L_{ON}) / 15] \quad \text{Eq. 1}$$

$$EOT = 9.87\,SIN\,2B - 7.53\,COS\,B - 1.5\,SIN\,B \quad \text{Eq. 2}$$

$$B = 360\,[(N - 81) / 364] \quad \text{Eq. 3}$$

Table 3 The conversion of the day Number

Month (Day)	Day Number, *N*	Notes
January (31)	d	d is the day of the month
February (28)	d + 31	
March (31)	d + 59	Add 1 when leap year
April (30)	d + 90	Add 1 when leap year
May (31)	d + 120	Add 1 when leap year
June (30)	d + 151	Add 1 when leap year
July (31)	d + 181	Add 1 when leap year
August (31)	d + 212	Add 1 when leap year
September (30)	d + 243	Add 1 when leap year
October (31)	d + 273	Add 1 when leap year
November (30)	d + 304	Add 1 when leap year
December (31)	d + 334	Add 1 when leap year
Days of Special Solar Interest		
Solar event	**Date**	**Day number, N**
Vernal equinox	March 21	80
Summer solstice	June 21	172
Autumnal equinox	September 23	266
Winter solstice	December 21	355

Note: Solstice and equinox dates may vary by a day or two. Also, add 1 to the solstice and equinox day number for leap years.

Source: John A. Duffie and William A. Beckman [18]

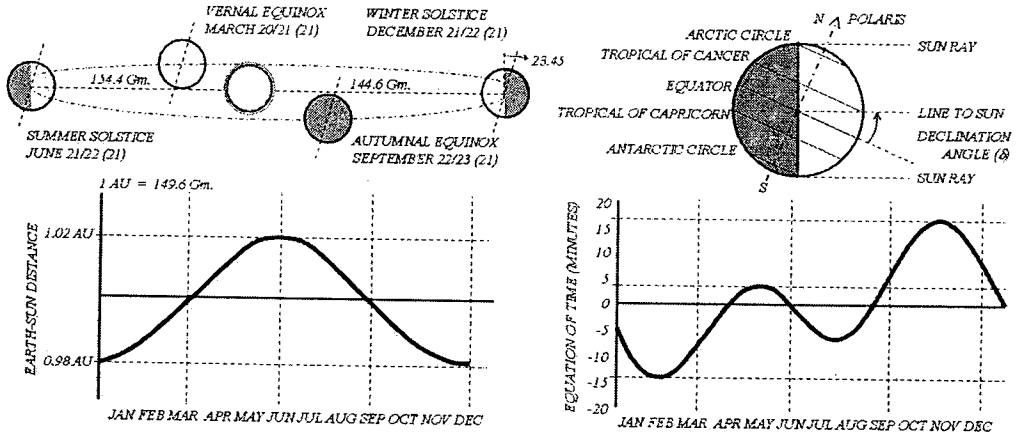

Figure 20 Orbit of the earth-sun and the equations of the relations

Source: American Society of Heating, Refrigerating and Air-Conditioning Engineers [2]; Kreider F. Jan and Curtiss S. peter [19]; William Stine and Michael Geyer [95]

2. Sun position

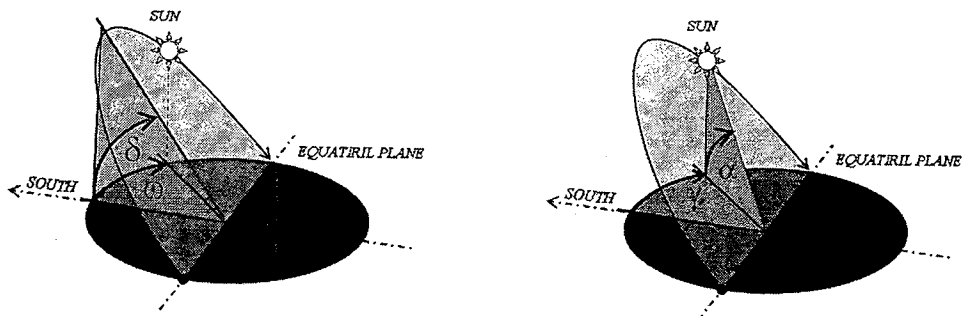

EQUATORIAL COORDINATE SYSTEM *ALT-AZ SYSTEM*

Figure 21 Co-ordinate systems of the Earth-Sun geometry

2.1 Equatorial coordinate system [19]

The coordinate system based on the celestial equator and the celestial poles are both defined in a similar manner to latitude and longitude on the surface of the earth, which is the equatorial coordinate system. This system defines the sun position with the hour angle that varies by the solar time and the declination angle that varies by the day number. Both are expressed as follows:

$$\omega = 15(t_S - 12) \quad \text{Eq. 4}$$

$$\delta = 23.45\ SIN\ [360(284 + N)/365] \quad \text{Eq. 5}$$

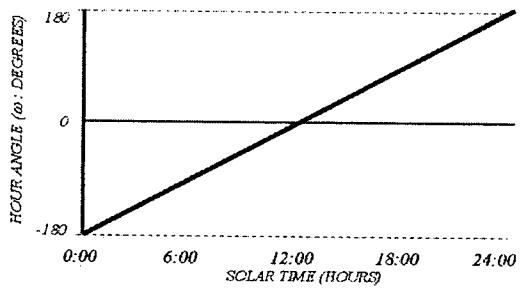

THE HOUR ANGLE COORDINATION

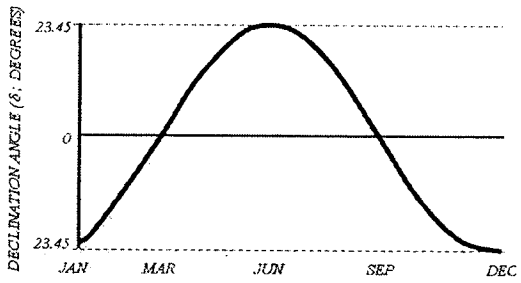

THE DECLINATION ANGLE COORDINATION

Figure 22 Co-ordinate system of the equatorial coordinate system

2.2 ALT-AZ system [19]

ALT-AZ system [19], a local coordinate system, defines the sun position with the solar altitude angle that varies by the latitude location, the declination angle and the hour angle. Another is the solar azimuth, which varies by the declination angle and the hour angle, also. These are expressed as follows:

$$\theta_Z = COS^{-1}(COS\ \phi\ COS\ \delta\ COS\ \omega + SIN\ \phi\ SIN\ \delta) \quad \text{Eq. 6}$$

$$\alpha = 90 - \theta_Z \quad \text{Eq. 7}$$

$$\gamma = SIN^{-1}(COS\ \delta\ SIN\ \omega / SIN\ \theta_Z) \quad \text{Eq. 8}$$

The sun path diagram is a tool used to design a shading device by specifying the altitude angle and the coordinates of time, such as the day and the solar time, in deciding the outstretched part of the shading device shown in both Figure 23 and Figure 24, which were simulated by Ecotect program.

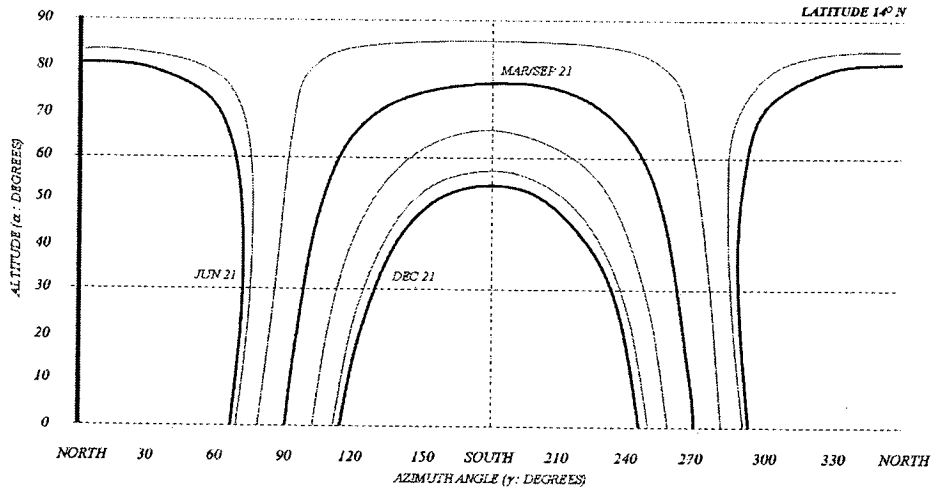

Figure 23 Co-ordinate system of the ALT-AZ system of the 14^{O} N latitude

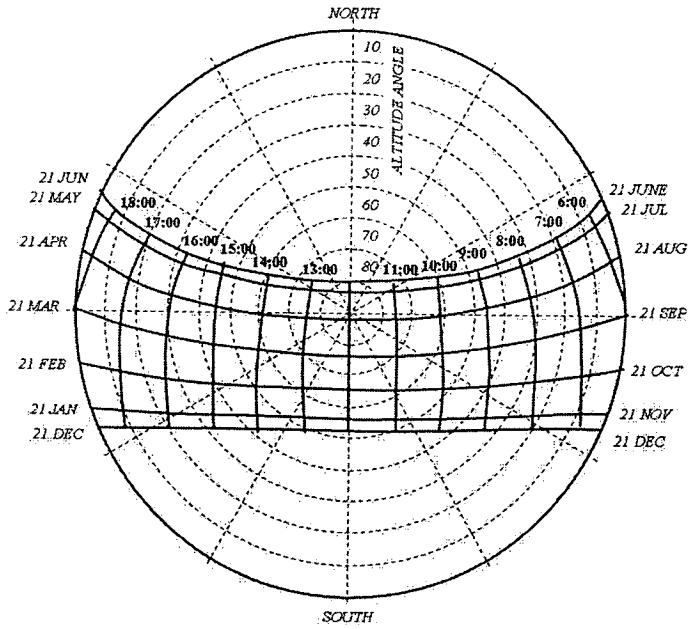

Figure 24 The sun path diagram of the 14^{O}N latitude

3. The extraterrestrial irradiance

Extraterrestrial irradiance is irradiance on a perpendicular plane outside the earth's atmosphere AM 0 with the constant of 1,367 W/m^2. It can be expressed by Eq.9 [2] as follows:

$$E_0 = 1{,}367\,[1 + 0.034\,COS\,(2\pi N / 365.25)] \qquad Eq.\ 9$$

4. Location parameter and hourly terrestrial irradiance

In Figure 18, the terrestrial irradiance on the earth's surface reduced by the mass of the atmosphere is divided into beam solar irradiance and diffuse solar irradiance from the sky presented by air mass (AM) definition as Eq. 10 [2]. The atmosphere is composed of dry air (such as N_2, O_2, and CO_2), inert gas, water vapor, and particles. This composition varies according to location and climate.

$$AM = SEC\ \theta_E \qquad \textit{Eq. 10}$$

The ratio of diffuse solar irradiance to total solar radiance is used to estimate diffuse solar irradiance using data collected by the weather station of location needed for estimation. Janjai, S., et al. [16] presented the relative functions between the ratios of the diffuse irradiance and the total irradiance in the form of the hourly clearness index, K, as follows in Eq.11-14

$$E_d / E_t = 0.8004 + 1.7153\,K - 7.3459\,K^2 + 5.5780\,K^3\ ;\ CM \qquad \textit{Eq. 11}$$

$$E_d / E_t = 0.6934 + 2.3406\,K - 8.0800\,K^2 + 5.6614\,K^3\ ;\ UB \qquad \textit{Eq. 12}$$

$$E_d / E_t = 0.7091 + 1.8910\,K - 6.2693\,K^2 + 3.9744\,K^3\ ;\ SK \qquad \textit{Eq. 13}$$

$$E_d / E_t = 0.6772 + 2.5680\,K - 8.8866\,K^2 + 6.3828\,K^3\ ;\ NP \qquad \textit{Eq. 14}$$

Note: CM is Chiang Mai province
UB is Ubon Ratchathani province
SK is Son khla province
NP is Nakhon Pathom province

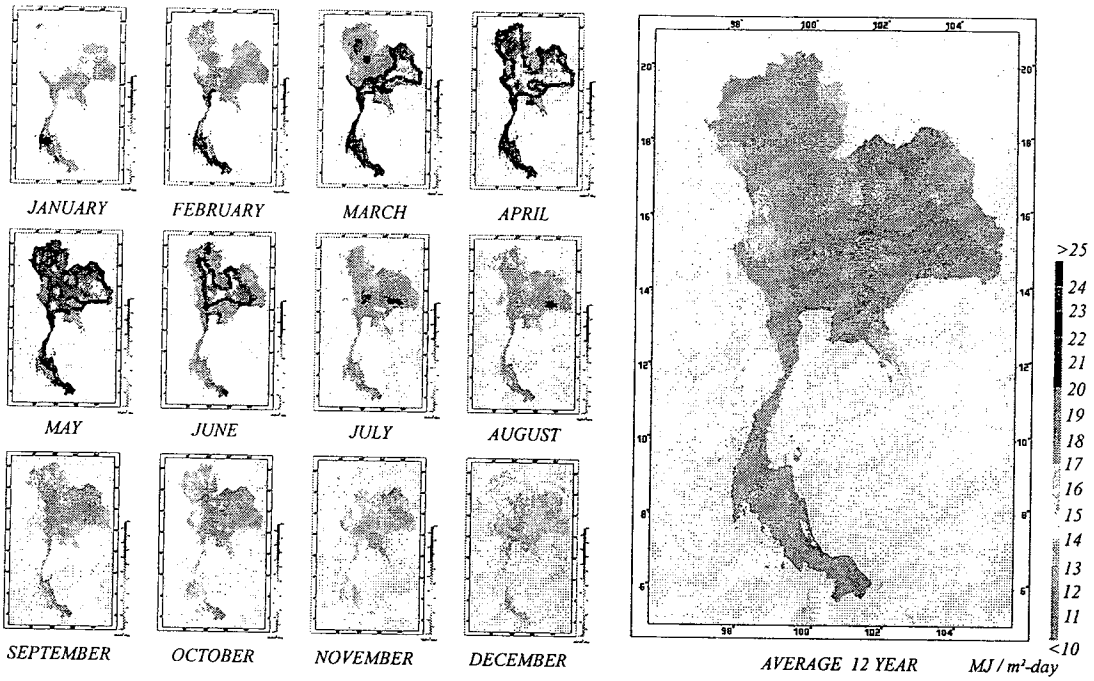

Figure 25 The solar maps of Thailand

Source: Department of Alternative Energy Development and Efficiency [65]

In Thailand, there is a solar map presentation by the Department of Alternative Energy Development and Efficiency (DEDE) and Faculty of Science, Silpakorn University [65] as shown in Figure 25.

5. Solar irradiance on the slope surface

ASHREA [2] presented the estimation of total irradiance on a slope surface shown in Eq.15 composing of the speech about beam solar irradiance, diffuse solar irradiance and ground reflected solar irradiance. However, the equation is based on a hypothesis named the isotropic sky model suggested by Hottel and Wortz (1942) and derived by Liu and Jordan (1963) as shown in Figure 26. However, the form of the anisotropic sky model is detailed in calculation more than the form presented by Hay and Davies (1980) consisting of horizontal sky term, the circum solar diffuse and the diffuse sky term. The form of the NDKR model (the Hay, Davises, Klucher, Reindl model) improved from the Hay and Davides model by Klucher (1979) and by Reindl, et al. (1990) had its composition divided further which is the horizontal sky term as shown in Figure 26.

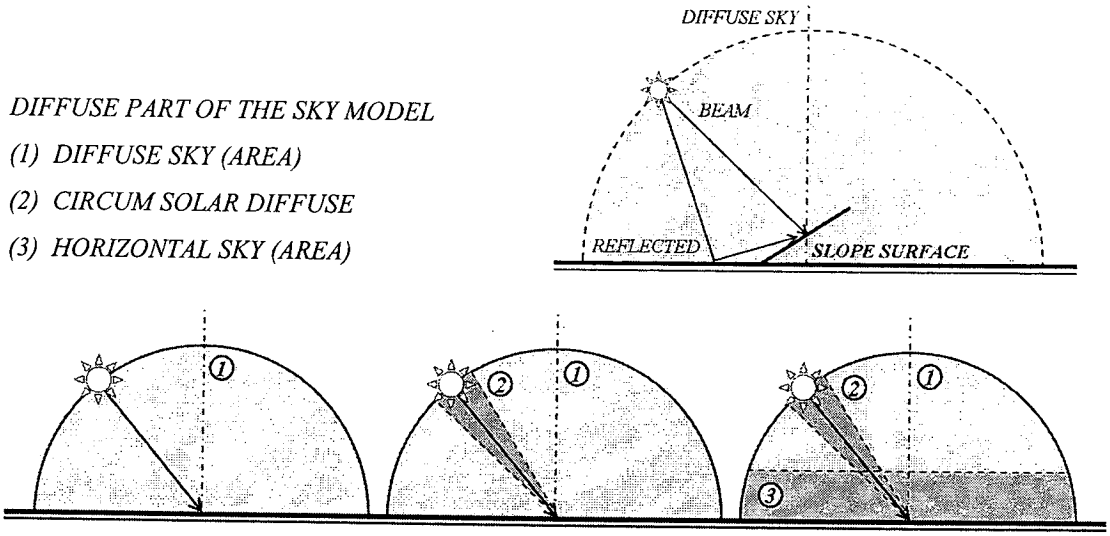

Figure 26 The comparison of sky models

Source: John A. Duffie and William A. Beckman [18]

The anisotropic sky model was tested in estimation. As a result, it has a higher value than the isotropic sky model by about 7%. Also, the estimation of HDKR model was higher than the isotropic sky model by about 9% with the test of the same instance. However, the isotropic sky model is simpler in trying to understand and estimate. ASHREA suggested that the circum solar diffuse and horizontal sky were not significant for annual energy performance calculations and Jan F. Kreider, et al. [19] suggested that the accuracy of the isotropic model will usually be sufficient for building. Where A_i is an anisotropic index, is an indicator of solar beam transmission getting through the earth's atmosphere.

$$E_{tS\text{-}ISO} = E_b R_b + E_d R_d + \sigma_g E_G R_{rG} \qquad \text{Eq. 15}$$

$$E_{tS\text{-}ANI} = (E_b + E_d A_i) R_b + (1 - A_i) E_d R_d + \sigma_g E_G R_{rG} \qquad \text{Eq. 16}$$

$$E_{tS\text{-}HDKR} = (E_b + E_d A_i) R_B + (1 - A_i) E_d R_d [1 + f SIN^3(\beta/2)] + \sigma_g E_g R_{gr} \qquad \text{Eq. 17}$$

$$R_b = COS\theta_i / COS\theta_Z \qquad \text{Eq.18}$$

$$R_d = (1 + COS\beta)/2 \quad \text{Eq. 19}$$

$$R_{rG} = (1 - COS\beta)/2 \quad \text{Eq. 20}$$

$$A_i = E_{DN} / E_O \quad \text{Eq. 21}$$

$$f = E_d / E_G \quad \text{Eq. 22}$$

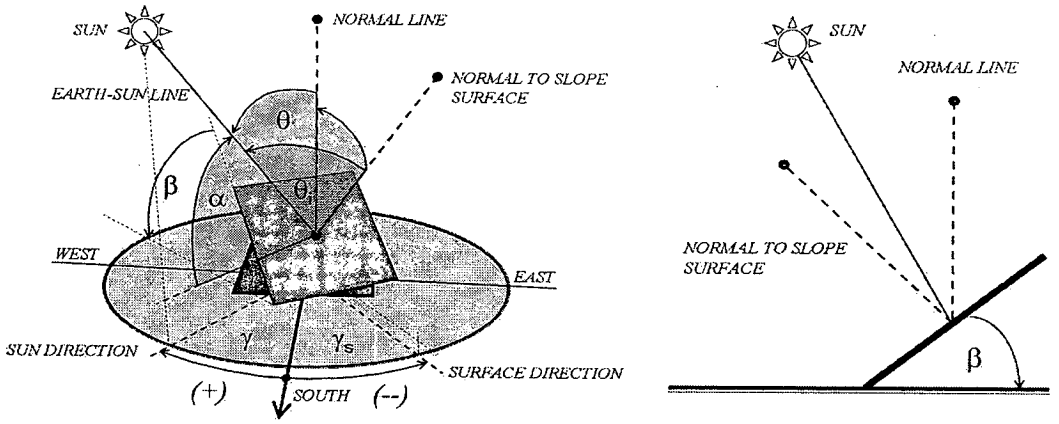

Figure 27 The geometry of earth-sun line on slope surface

Source: American Society of Heating, Refrigerating and Air-Conditioning Engineers [2]

ASHREA [2] presented equations such as Eq. 23-32 with variables A, B and C as determination of the solar irradiance intensity containing the A, B and C values shown in Table 4.

$$E_{tS} = E_{DN} COS\theta_i + E_d + E_{rG} \quad \text{Eq. 23}$$

$$E_{DN} = A / exp\,(B / SIN\alpha) \quad \text{Eq. 24}$$

$$Y = 0.55 + 0.437\, COS\theta_i + 0.313\, COS^2\theta_i \;;\; COS\theta_i > -0.2 \quad \text{Eq. 25}$$

$$Y = 45 \qquad ;\; COS\theta_i <= -0.2 \quad \text{Eq. 26}$$

$$E_d = CYE_d \qquad ;\; \text{Vertical surface} \quad \text{Eq. 27}$$

$$E_d = CYE_d\,[(1 + COS\beta) / 2] \qquad ;\; \text{Other slope} \quad \text{Eq. 28}$$

$$E_{rG} = E_{DN}\,[(C + SIN\alpha)\rho_g\,[(1 - COS\beta) / 2] \quad \text{Eq. 29}$$

$$COS\theta_i = SIN\delta\, SIN\phi\, COS\beta - SIN\delta\, COS\phi\, SIN\beta\, COS\gamma + COS\delta\, COS\phi\, COS\beta\, COS\omega + COS\delta\, SIN\beta\, SIN\gamma\, SIN\,\omega + COS\delta\, SIN\phi\, SIN\beta\, COS\gamma\, COS\omega \quad \text{Eq. 30}$$

$$COS\theta_i = SIN\theta_Z\, SIN\beta\, COS(\gamma_S - \gamma) + COS\theta_Z\, COS\beta \quad \textit{Eq. 31}$$

$$COS\theta_Z = COS\phi\, COS\delta\, COS\omega + SIN\phi\, COS\delta \quad \textit{Eq. 32}$$

Table 4 The relative data of extraterrestrial irradiance (the base year of 1964)

Month	E_0	EOT	Declination	A	B	C
(21st day)	W/m²	min	degrees	W/m²	Dimensionless ratio	
Jan	1416	−11.2	−20.0	1230	0.142	0.058
Feb	1401	−13.9	−10.8	1215	0.144	0.060
Mar	1381	−7.5	0.0	1186	0.156	0.071
Apr	1356	1.1	11.6	1136	0.18	0.097
May	1336	3.3	20	1104	0.196	0.121
June	1336	−1.4	23.45	1088	0.205	0.134
July	1336	−6.2	20.6	1085	0.207	0.136
Aug	1338	−2.4	12.3	1107	0.201	0.122
Sep	1359	7.5	0.0	1151	0.177	0.092
Oct	1380	15.4	−10.5	1192	0.16	0.073
Nov	1405	13.8	−19.8	1221	0.149	0.063
Dec	1417	1.6	−23.45	1233	0.142	0.057

For Thailand radiation data at the Bangkok station, 14°N latitude, during year 2009 was practiced estimation using ASHREA's equation determining reflectance of general ground surface at 0.2 [2] as shown in Figure 28. It was found that maximum solar radiation was 1,840 kW/ m^2 -Year at a slope surface of 20 degrees turning south. It decreased more than half when the slope at the angle was 70 degrees turning north between NW and NE.

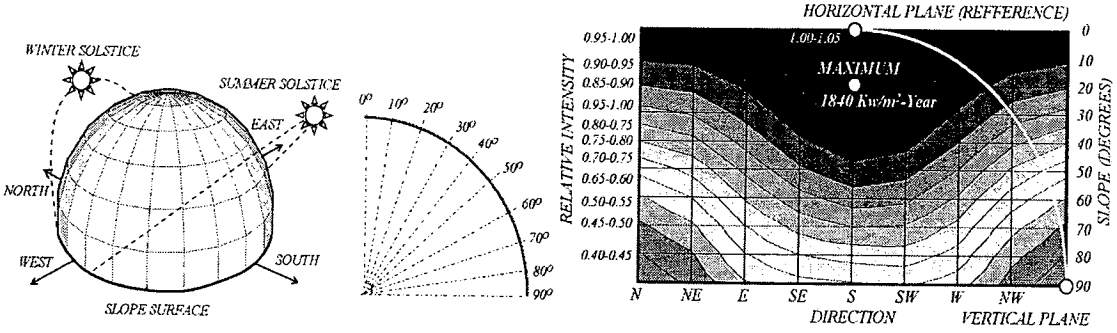

Figure 28 The relative intensity of annual solar irradiance of Thailand

Table 5 The relative intensity of annual solar irradiance on surface of Thailand

Slope	Direction							
(degrees)	N	NE	E	SE	S	SW	W	NW
Global	1.000	1.000	1.000	1.000	1.000	1.000	1.000	1.000
10	0.960	0.966	0.987	1.010	1.023	1.017	0.996	0.973
20	0.904	0.917	0.959	1.003	1.028	1.016	0.977	0.930
30	0.834	0.856	0.918	0.981	1.015	0.999	0.943	0.874
40	0.753	0.788	0.869	0.943	0.984	0.966	0.899	0.810
50	0.667	0.718	0.814	0.892	0.937	0.919	0.848	0.742
60	0.595	0.651	0.756	0.832	0.875	0.861	0.791	0.675
70	0.540	0.593	0.700	0.767	0.801	0.795	0.734	0.615
80	0.496	0.546	0.646	0.699	0.719	0.726	0.678	0.565
90	0.464	0.510	0.595	0.635	0.645	0.658	0.623	0.527

Note: initial data, global solar irradiance and diffuse solar irradiance collected hourly by TMD summed as the total 1,788 kW/m^2-Year that was compared with the estimated by the same process as the total 1,789 kW/m^2-Year, which was closely.

6. Solar irradiance on the tracking surface

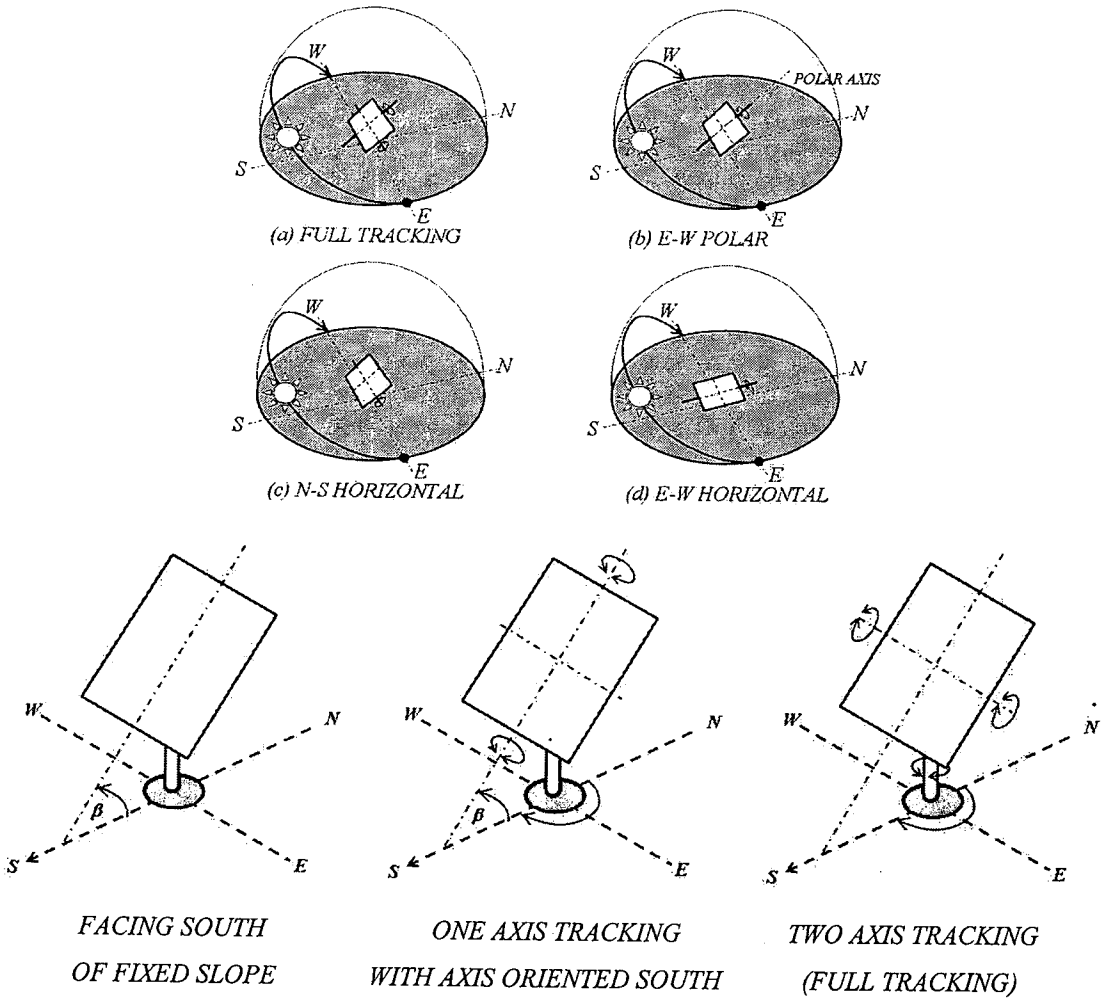

Figure 29 The type of PV tracking systems

Source: Magal, B.S. [22]

Tracking is the movement of the incident angle separated according to the pattern shown in Figure 29

6.1 Two axis tracking (a) [18, 22]

This movement function keeps the face to the sun at all times, as in Eq. 33.

$$COS\theta_i = 1 \qquad \text{Eq 33}$$

6.2 Fixed tilted with E-W tracking

6.2.1 Tilted N-S axis with tilted adjusted daily (like b) [18, 22]

The surface is a fixed slope on the N-S axis and rotated with the E-W axis, as in Eq.34 and the slope as in Eq.35.

$$COS\theta_i = SIN^2\delta + COS^2\delta COS\omega \qquad Eq.\ 34$$

$$\beta = |\phi - \delta|,\ if\ (\phi - \delta) > 0,\ \gamma_S = 0\ or\ if\ (\phi - \delta) < 0,\ \gamma_S = 180 \qquad Eq.\ 35$$

6.2.2 Polar N-S axis with E-W tracking (b) [18, 22]

The surface is a fixed slope on the N-S axis parallel to the axis of the earth, as in Eq. 36 and the slope as in Eq.37.

$$COS\theta_i = COS\delta \qquad Eq.\ 36$$

$$TAN\beta = TAN\phi / COS\gamma_S \qquad Eq.\ 37$$

6.3 Horizontal with tracking

6.3.1 Horizontal E-W axis with N-S tracking (c) [18, 22]

This movement is fixed parallel with the earth and tracking daily with the N-S axis, as in Eq. 38 of Duffie and Beckman (1991) and Eq. 39 of Meinel and Meinel (1976).

$$COS\theta_i = (1 - COS^2\delta SIN^2\omega)^{0.5} \qquad Eq.\ 38$$

$$COS\theta_i = ((SIN^2\delta + COS^2\delta COS^2\omega)^{0.5} \qquad Eq.\ 39$$

$$TAN\beta = TAN\theta_Z / |COS\gamma|\ ,\ if\ \gamma < 90,\ \gamma_S = 0\ or\ if\ \gamma > 90,\ \gamma_S = 180 \qquad Eq.\ 40$$

6.3.2 Horizontal N-S axis with E-W tracking (d) [18, 22]

This movement is fixed parallel with the earth and tracking all day with the E-W axis, as in Eq. 41 of Duffie and Beckman (1991) and Eq. 42 of Meinel and Meinel (1976) and slope as in Eq. 43.

$$COS\theta_i = (COS^2\theta_Z + COS^2\delta SIN^2\omega)^{0.5} \quad Eq.\ 41$$

$$COS\theta_i = COS\phi\, COS\omega + COS\delta SIN^2\omega \quad Eq.\ 42$$

$$TAN\beta = TAN\theta_Z / COS(\gamma_S - \gamma) / \ , if\ \gamma > 0,\ \gamma_S = 90\ or\ if\ \gamma < 0,\ \gamma_S = -90 \quad Eq.\ 43$$

The comparison is estimated for 35° latitude with standard conditions shown in Figure 30

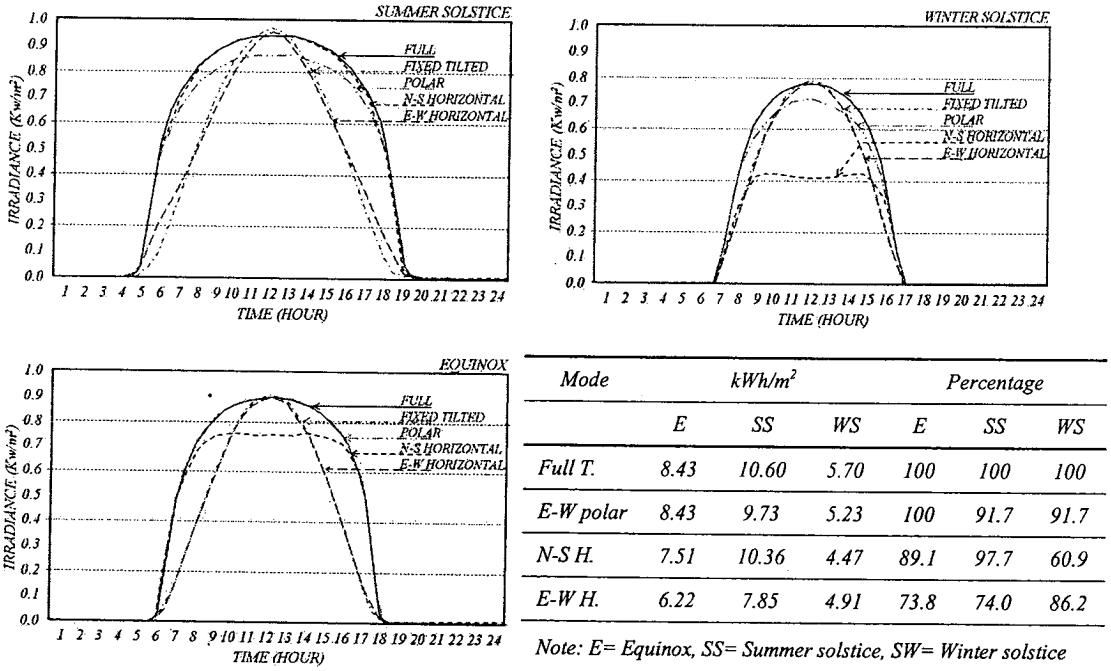

Mode	kWh/m²			Percentage		
	E	SS	WS	E	SS	WS
Full T.	8.43	10.60	5.70	100	100	100
E-W polar	8.43	9.73	5.23	100	91.7	91.7
N-S H.	7.51	10.36	4.47	89.1	97.7	60.9
E-W H.	6.22	7.85	4.91	73.8	74.0	86.2

Note: E= Equinox, SS= Summer solstice, SW= Winter solstice

Figure 30 The solar irradiance of PV tracking systems

Source: Magal, B.S. [22]

Photovoltaic power system

This section reviews the energy produced by the photovoltaic system to be integrated with a shading device, which is a system used to convert the solar radiation as it is the heat source of air conditioning systems into electricity energy.

1. PV materials

The photoelectric process in semiconductor material studied and developed as many kinds of photovoltaic technologies can be ranged as shown in Figure 31. Composition of a PV module is shown in Figure 32. Well-developed technologies such as crystalline and amorphous silicon made up 85% of the market share. Both are made of silicon but with different procedures. One problem of PV technology was low efficiency conversion, so it was designed to have a composition that reduces received solar energy loss, for example, glass can be put on top of the solar module to trap light or reduce the degree of reflection with AR coating as shown in Figure 32.

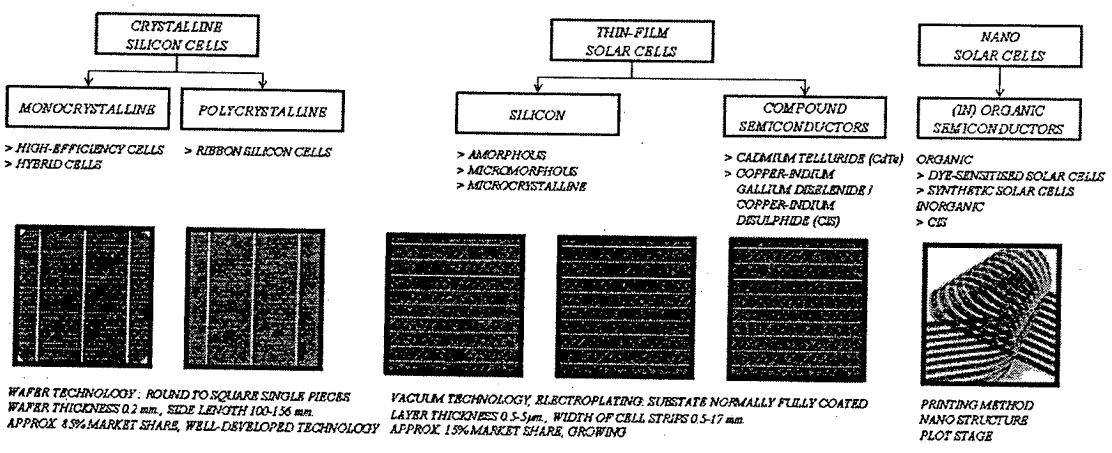

Figure 31 The classification of PV technologies

Source: Bernhard Weller, Claudia Hemmerle, Sven Jakubetz and Stefan Unnewehr [5]

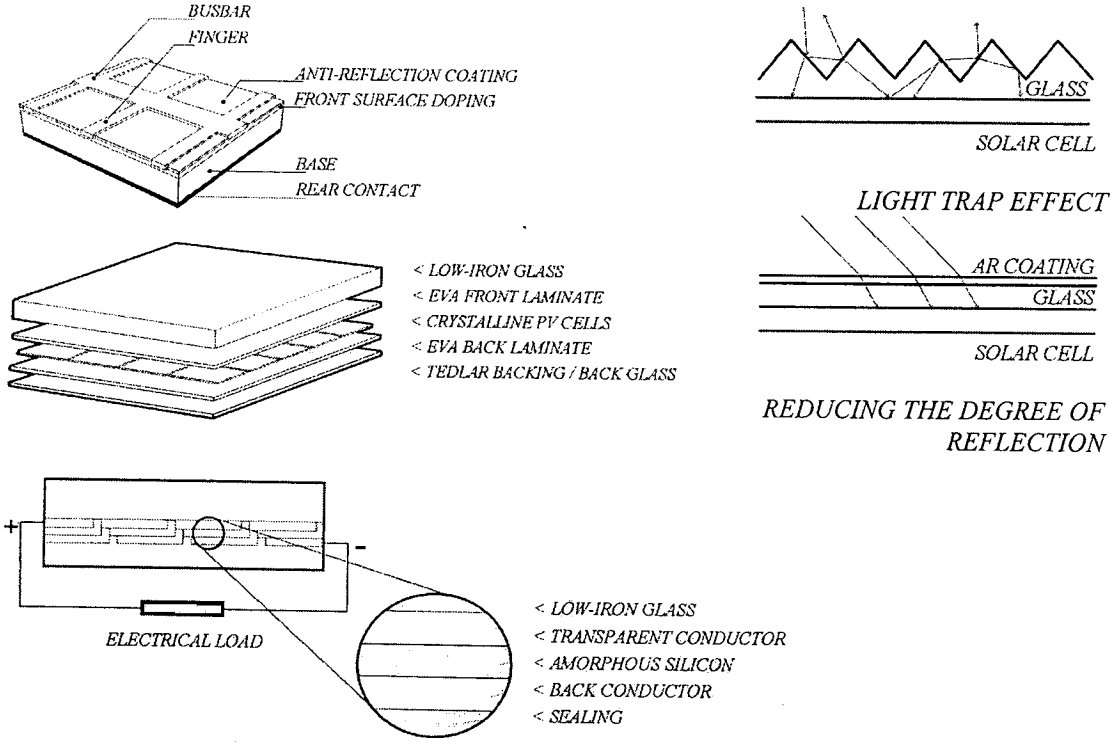

Figure 32 The components of PV module

Source: Bernhard Weller, Claudia Hemmerle, Sven Jakubetz and Stefan Unnewehr [5]; Simon Roberts and Nicolo Guariento [27]

2. PV module efficiency

PV modules are used in the production of electricity from light; it is a clean and renewable energy source. The conversion is caused from electrons and holds diffuse between the P-N junction depending on the energy band gap. However, the solar energy falling on the PV surface cannot convert to the electrical energy all, so the technology has low efficiency.

2.1 Spectral sensitivity

The efficiency of PV cells resulted from components of crystalline cells responding to the spectrum in a long-wave period better than thin-film cells. However, it responds less in a period of visible light as shown in Figure 33. C. Titiporn [54] found that in Thailand's climate, both technologies respond to energy production according to conditions of the sky, which change seasonally. Figure 34 shows the data collection for the study at SERT for 4 years.

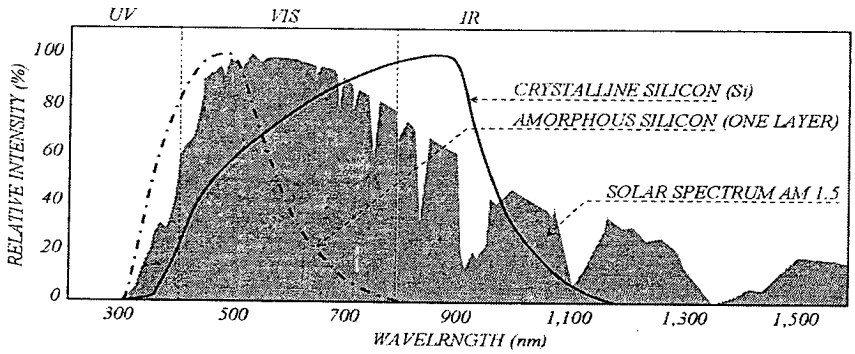

Figure 33 The relative intensity of PV materials

Source: Bernhard Weller, Claudia Hemmerle, Sven Jakubetz and Stefan Unnewehr [5]; Sterling, VA. [30]

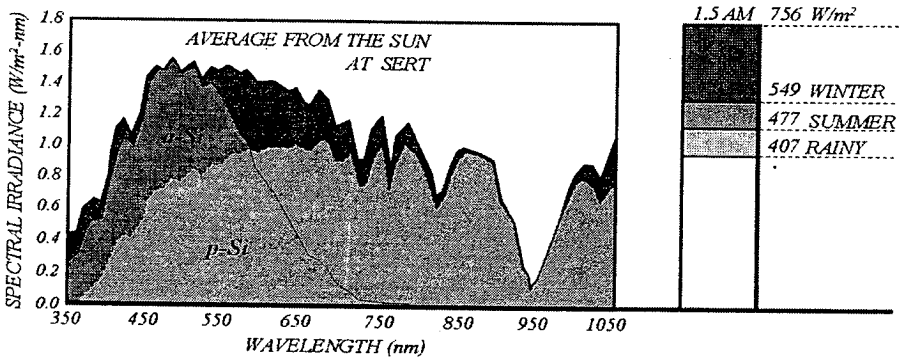

Figure 34 The responsive spectral irradiance of p-Si and a-Si in Thailand

Source: Bernhard Weller, Claudia Hemmerle, Sven Jakubetz and Stefan Unnewehr [5]

2.2 I-V curve characteristic and fill factor

Identity of PV was explained by the relation in the form of I-V curve (the character of PV unit can be expressed in the curve of I and V relationship) indicating efficiency and performance of each PV cell. It was tested using Standard Test Conditions (STC) such as module temperature at 25°C, solar irradiance on cell surface at 1,000 W/m^2 and 1.5 AM, or according to outdoor conditions determined by normal operating cell temperature (NOCT) conditions such as at 20° C, irradiance on cell surface at 800 W/m^2, wind velocity of 1.0 m/s and open back-side mounting.

Fill factor, FF, shown in Figure 35, in which proportion is reduced by the characteristic series resistance and shunt resistance affecting efficiency of a PV cell were able to be explained by using Eq. 44-47. FF of poly crystalline silicon and amorphous silicon was approximately 0.75-0.85 and 0.56-0.61, respectively [30].

$$\eta = P_o / P_i \qquad \text{Eq. 44}$$

$$= P / E_{tS} A_{PV} \qquad \text{Eq. 45}$$

$$= FF\, I_{SC}\, V_{OC} / P_i \qquad \text{Eq. 46}$$

$$FF = P_{MP} / I_{SC}\, V_{OC} \qquad \text{Eq. 47}$$

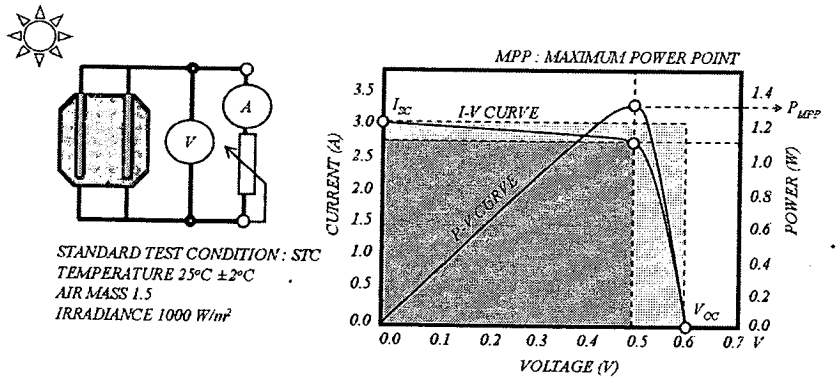

Figure 35 The curve characteristic and fill factor

Source: Simon Roberts and Nicolo Guariento [27]; Sterling, VA. [30]

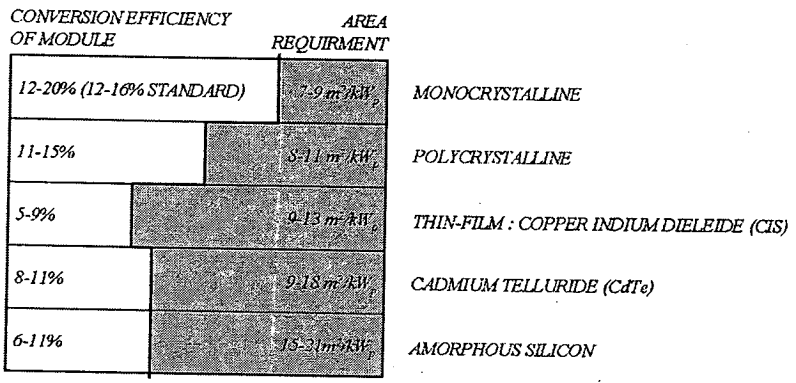

Figure 36 The conversion efficiency of module technologies

Source: Simon Roberts and Nicolo Guariento [27]; Sterling, VA. [30]

As for installation, the surface area of the panels is very impotent due to the limited area of the building surface and limited area suitable for solar radiation reception.

2.3 Module temperature effect

The diode model expressed in Eq. 48 [68] showed current: I which was varied according to cell temperature and voltage: V_{oc}. It also decreased with higher levels of temperature cell as shown in Eq. 49 [68].

$$I = I_0 [exp(qV/nkT) - 1] - I_L \qquad Eq.\ 48$$

$$V_{OC} = (kT/q)\ ln\ (I_{SC} / I_0) \qquad Eq.\ 49$$

Note: at 300.00 K (26.85°C), kT/q = 25.850 mV, the thermal voltage. at 298.15 K (25.00°C), kT/q = 25.693 mV

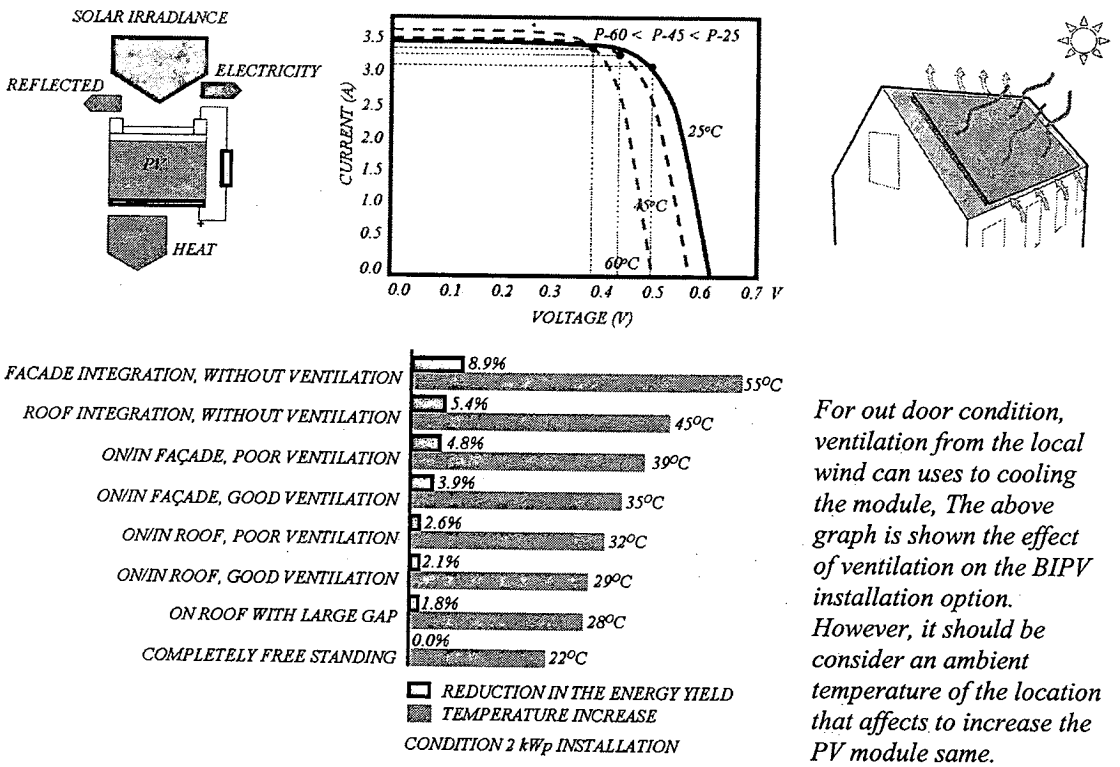

For out door condition, ventilation from the local wind can uses to cooling the module, The above graph is shown the effect of ventilation on the BIPV installation option. However, it should be consider an ambient temperature of the location that affects to increase the PV module same.

Figure 37 The module of temperature effect

Source: Simon Roberts and Nicolo Guariento [27]; Sterling, VA. [30]

The open circuit voltage slightly constant decrease as the irradiance change when the irradiance fall below 100 W/m^2 does the voltage break down and rapidly decrease, which likes the overcast sky condition.

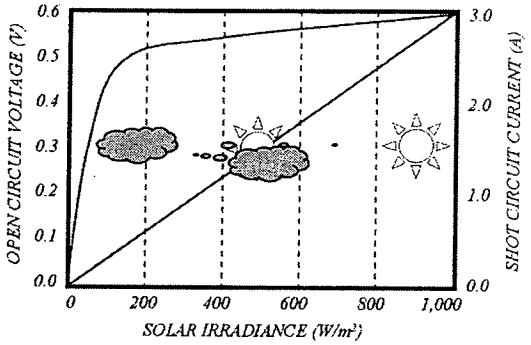

Figure 38 The sky condition and the PV electrical characteristics

Source: Sterling, VA. [30]

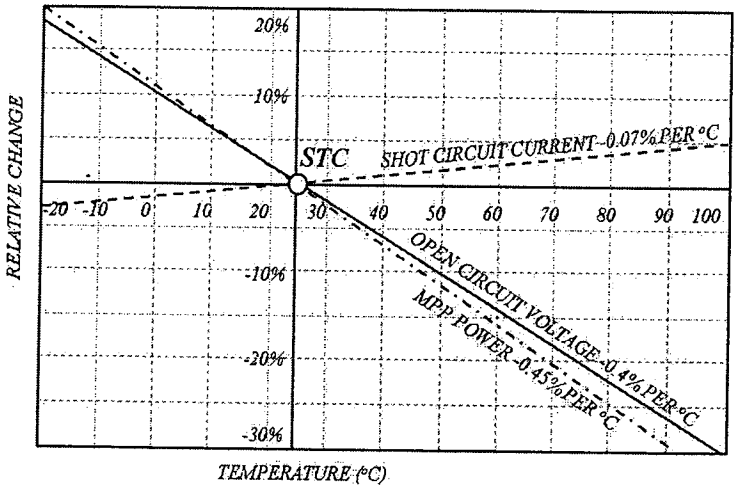

TEMPERATURE COEFFICIENT (% /°C)

CRYSTALLINE SILICON
-0.4 TO -0.5

AMORPHOUS SILICON
-0.21

CADMIUM TELLURIDE (CdTe)
-0.25

COPPER INDIUM GALLIUM SELENIDE (CIGS)
-0.32 to 0.36

Figure 39 The relative change of PV parameters

Source: Energy Market Authority and Building and Construction Authority [12]; Sterling, VA. [30]

The PV array, the group of PV modules, was installed on the roof or building surface, causing less ventilation than standalone PV array installation. It is the same as shading device installation. However, if a photovoltaic system were designed to be integrated into the system in a form of shading device, it would create better ventilation around the PV module. A comparison of the differences is shown in Figure 37.

3. The losses of PV system

Figure 40 illustrates the average the losses of a sample BIPV system and the temperature effects of different installations. In the case of a CIS warm façade, loss because of temperature was about 6% with no shadow effect. Roof-mounted installation losses due to temperature were about 3.5% and 2% from shadow effect. According to study cases, the most loss was from inverter operation was 10% and 7% respectively.

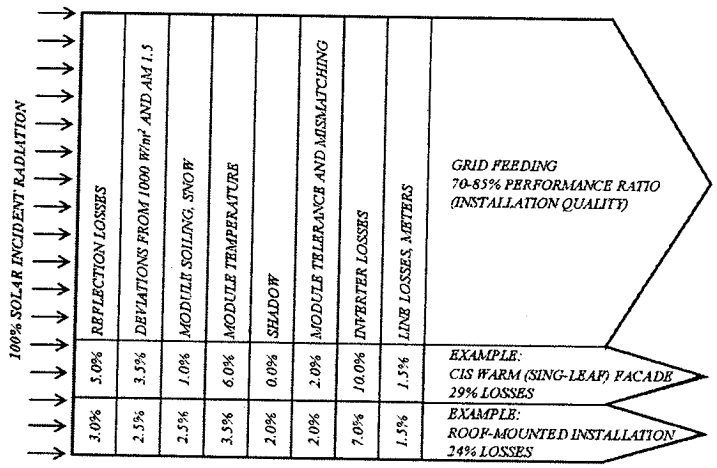

Figure 40 The energy loss and performance ratio for the PV installations

Source: Jesse Henson [17]

3.1 Shadow effect

For BIPVs in the city received partial shade on the PV cell connection shown in Figure 41 affected current or volt reduction according to cell connection.

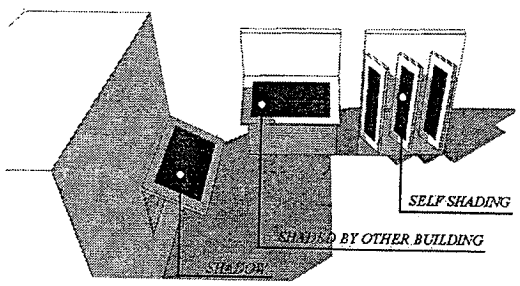

Figure 41 Shading effect on PV module

3.2 Degradation and Failure Modes

Degradation is a parameter that shows the stability and resistance to corrosion of the materials affecting the decreased efficiency or less electricity producing capacity of system operation or. Normally, the manufacturer guarantee is set at 20 years, which indicates the quality of bulk silicon PV modules currently being produced.

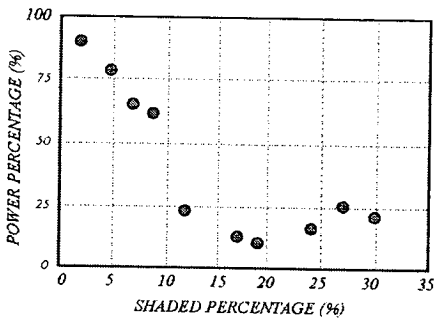

Hot-Spot Failures
Mismatched, cracked or shaded cells can lead to hot-spot failures, as discussed previously in Hot Spot Heating.

Figure 42 The relation of shading on the PV array and PV power

Source: Deo Prasad and Mark Snow [10]

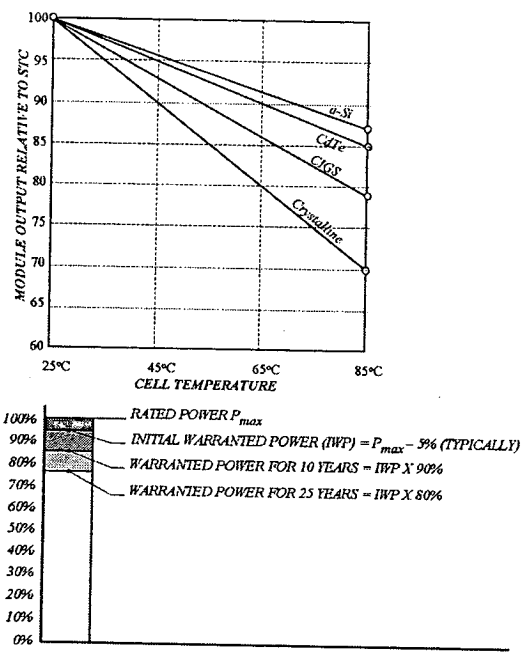

Technologies	*Temperature Coeficiency (%/°C)*
Crystalline	*-0.40 to -0.45*
CIGS	*-0.32 to -0.36*
CdTe	*-0.25*
a-Si	*-0.21*

Figure 43 The PV efficiency drop

Source: Building and Construction Authority [63]

PV modules produces under STC have a limited power output warranty. Most manufacturers guarantee at least 90% of the minimum rated output for 10 years and 80% of the minimum rated output for 20-25 years. It should be noted that the minimum rated output is usually defined as 95% of the rated output to allow for manufacturing and measurement tolerances, which is illustrated in Figure 43.

3.3 Inverter efficiency

The inverter is the element in charge of converting electricity produced by the PV system and connects with the parallel or series PV module as shown in Figure 44. This component works under weather conditions affecting the efficiency depending on the severity of radiation. B. Tharika [53] found that 40% of energy content was produced from solar irradiance between 720 and 960 W/m^2 and 92% of the efficiency of the inverter for operation under Thailand radiation was more than 90%. However, energy content in solar irradiance between 0-350 W/m^2, which was a period of diffuse irradiance, created inverter efficiency at 20% causing negative results towards electrical energy production, as shown in Figure 45.

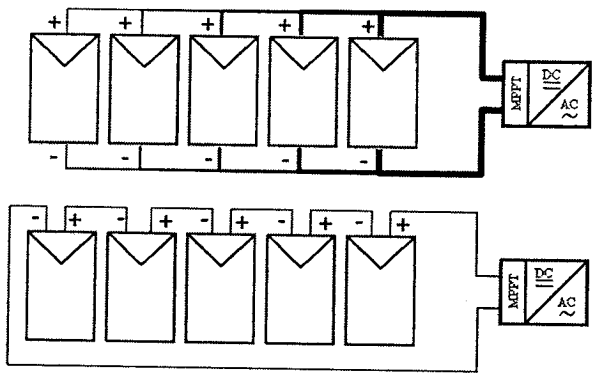

< Parallel connection

< Series connection

Figure 44 The connection of PV modules with an inverter

Source: Simon Roberts and Nicolo Guariento [27]

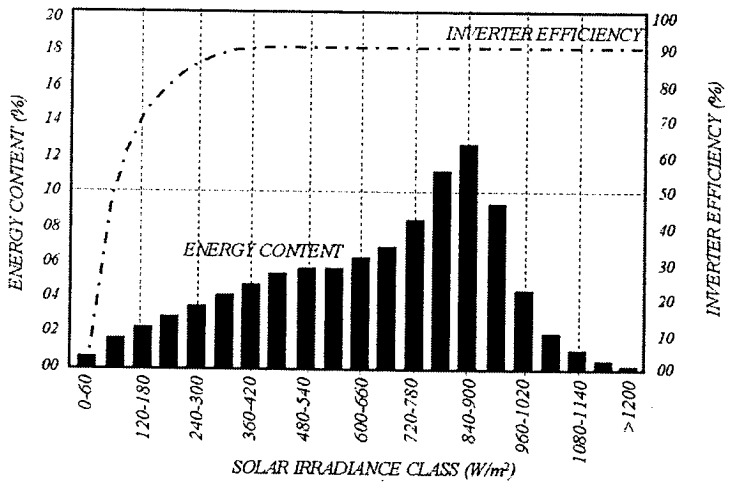

Figure 45 The comparison of the energy content and inverter efficiency

Source: Bunphan, Tharika [53]

4. BIPV design and installation

4.1 Construction and integration

A roof-mounted PV construction system is generally found functioning only as additional electrical energy production not for protection from the weather. The alternative is to place the module within the building envelope with the same function. For example, the function of a PV installation is to be weather proof cladding installed on the external wall. It is a design consideration in the case of a cold (double-leaf) façade and an integration option to create the highest level of benefit in regards to materials and construction. Its functions are weather protection, thermal insulation, sun shading and sound insulation. Therefore, it is an attractive choice for building design.

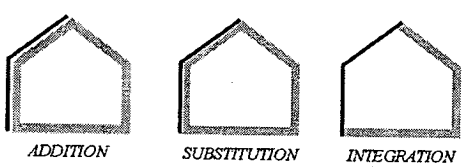

Figure 46 The constructional integration of building

Source: Bernhard Weller, Claudia Hemmerle, Sven Jakubetz and Stefan Unnewehr [5]

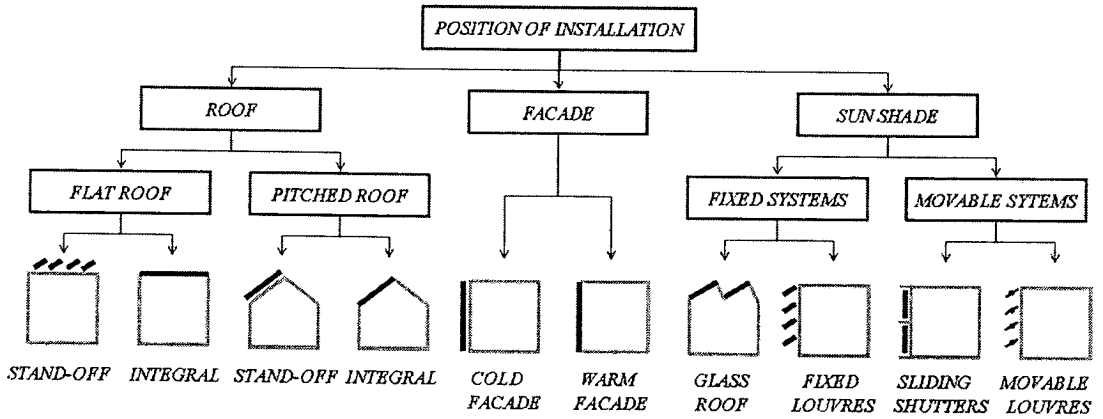

Figure 47 The principal installation options

Source: Bernhard Weller, Claudia Hemmerle, Sven Jakubetz and Stefan Unnewehr [5]

Integration as sun shade is classified into two types as illustrated in Figure 47. The fixed system is designed as a glass roof to decrease light coming into the building, which is good for daylight. Fixed louvers help in reducing heat coming into the building, which is good for thermal. In addition, movable systems are designed to control light and heat coming in the building using smaller modules.

Figure 48 describes the beneficial functions of transparent PV modules, which are generating, shading and lighting. Transparent PV options are used because of the need for daylight, causing the PV element to be more beneficial than just producing electricity, as shown in Figure 48. However, transparent PV cells had been developed from organic technology with less than 1.0% efficiency. Not long after that, MIT's team developed its efficiency to be 1.7% in the early-prototype solar cells [82].

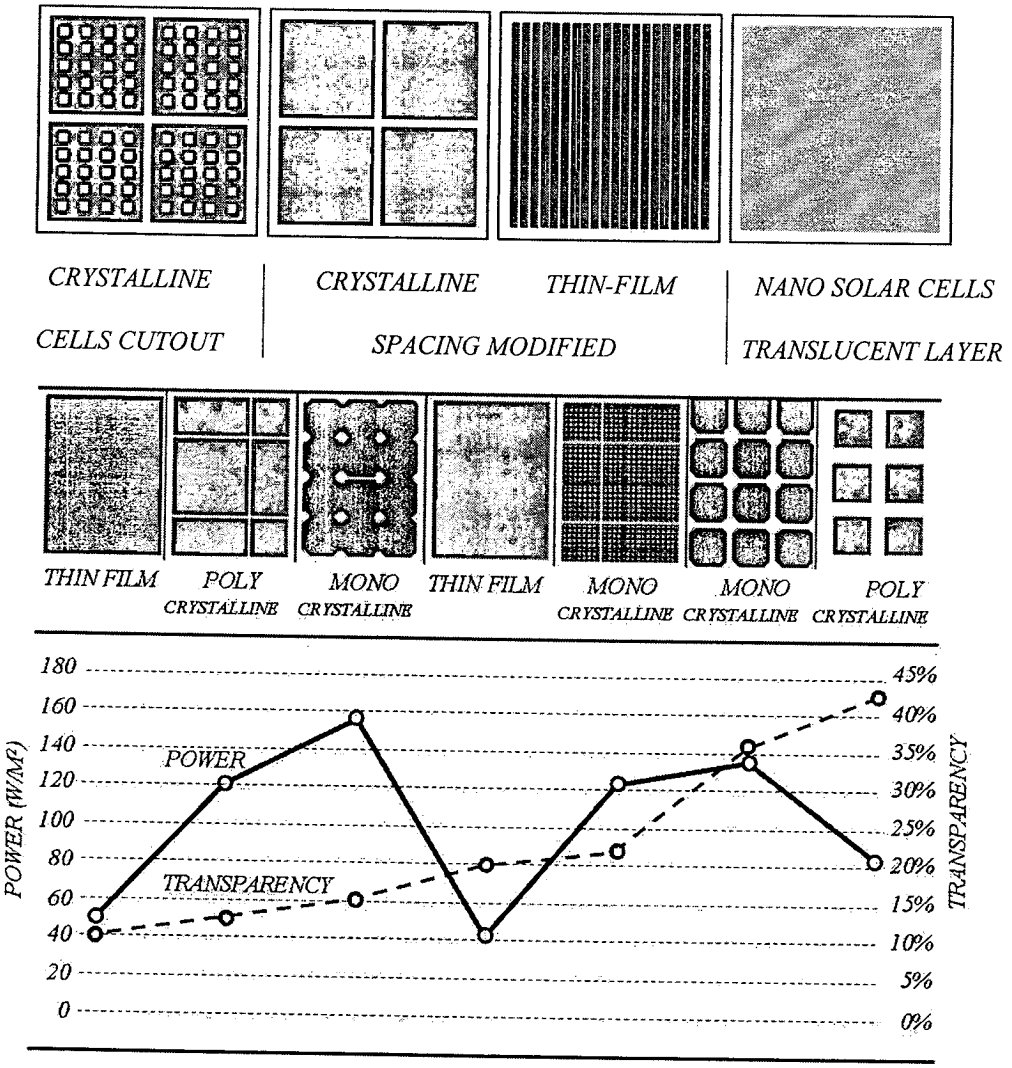

Figure 48 The types of transparent PV module

Source: Sapa build ing system ab offices [83]

4.2 BIPV potential in city

Performance of PV is considered low if installed is in the city. This is a result of the shade from the high buildings around the modules. Nevertheless, there are the cases of tall dominant buildings having no block. Figure 49 shows the different results between BIPV installed on the roof and BIPV installed on a façade. It was found that a tilted angle of the roof gained more benefit than a tilted angle of the façade or vertical wall.

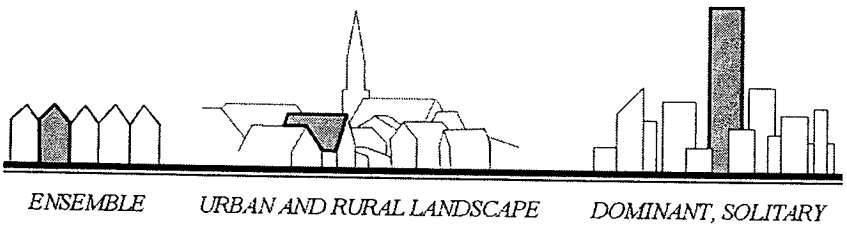

Figure 49 The relation between PV and the surroundings

Source: Bernhard Weller, Claudia Hemmerle, Sven Jakubetz and Stefan Unnewehr [5]

Table 6 Rules of thumb for BIPV potential

Solar architectural rules of thumb for BIPV potential			
	on ROOF		on FAÇADE
Ground floor area	1 m^2	Base of BIPV potential in relative terms	1 m^2
Gross area	1.2 m^2	Ratio gross area / ground floor area	1.5 m^2
	60%	Suitable building envelope parts taking in to account construction, historical and shading elements, including vandalism factor	20 %
Architecturally Suitable area	0.72 m^2	Ratio architecturally suitable area / ground floor area	0.3 m^2
	55%	Suitable building envelope parts taking into account sufficient solar yield	50 %
Solar architecturally Suitable area	0.4 m^2	Ratio solar architecturally suitable area / ground floor area (Utilisation factor)	0.15 m^2

Source: Deo Prasad and Mark Snow [10]

5. Case study of shading integrated

5.1 Installation case study

5.1.1 Galleria Naviglio

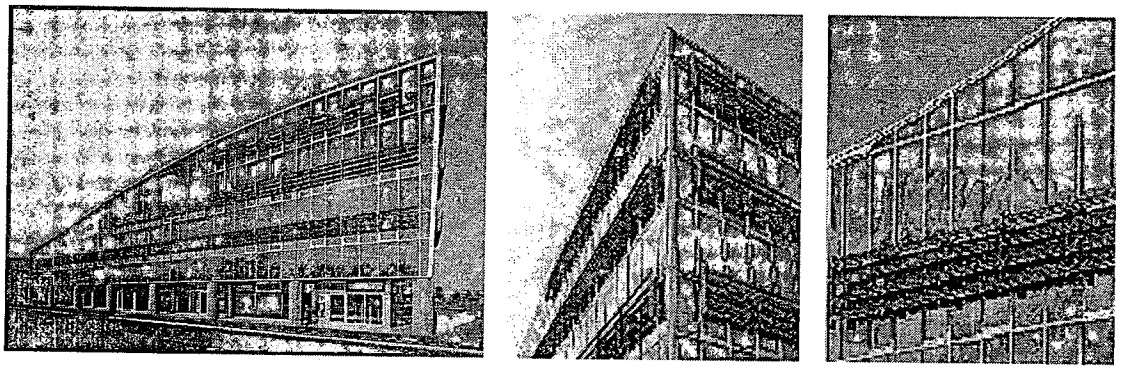

Complex office, shops, apartment, Faenza, Italy (latitude 44.3°N)

PV installation type : Mono crystalline

Shading Type tilted 70° azimuth South East and North East

Total 21 kW_p η-PV array 7.8% – 9.2%, η-PV system 7.0 – 8.2 PR 34%

PR 33.88% (Estimation)

Figure 50 Photovoltaic system of Galleria Naviglio

Source: Simon Roberts and Nicolo Guariento [27]

5.1.2 Photovoltaic System Research Center

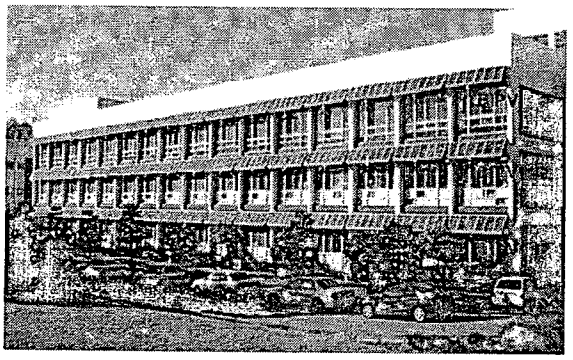

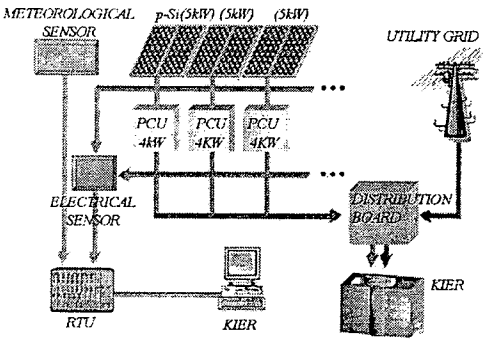

Korea Institute of Energy Research, Taejeon, South Korea (latitude 36°N)

PV installation type : Poly crystalline (50 W_p module)

Shading Type tilted 60° azimuth -10 degrees (South East)

Total 15.00 kW_p η-PV array 7.8% – 9.2%, η-PV system 7.0 – 8.2 PR 65% – 76%

3th Floor 5.28 kW_p PR 76.1%

2nd Floor 4.87 kW_p PR 70.1%

1st Floor 4.48 kW_p PR 65.3%

Figure 51 Photovoltaic system of Research Center

Source: Yu, G.J., So, J.H., Jung, Y.S., Kang, G.H. and Choi, J.Y. [52]

5.1.3 Samsung Institute of Engineering and Construction Technology

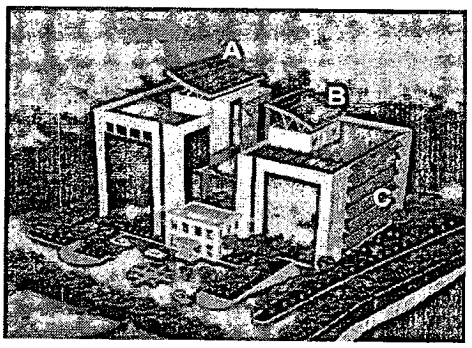

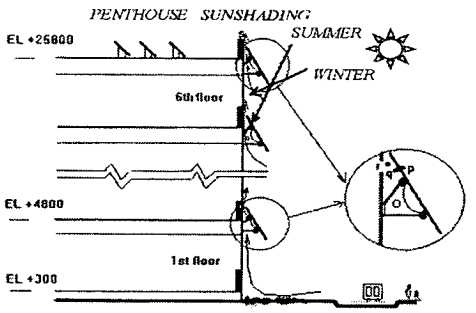

ELEVATION

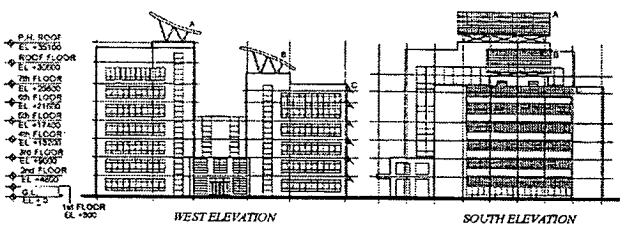

RISER DIAGRAM

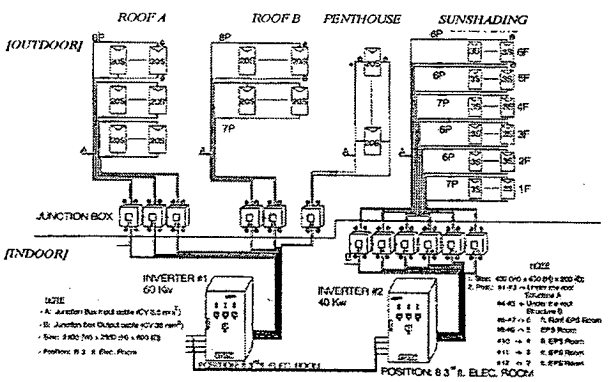

Korea Institute of Energy Research, Taejeon, South Korea (latitude 37.3°N)

PV installation type : Mono crystalline

Shading Type tilted 55.5°(for aesthetic) azimuth 0 degrees (South)

Total 40 kW_p (C : shading) η-PV module 14% , PR 25% – 40% (PR of Array yielded)

Cloudy day PR 40.59% module temperature 27.6°C

Normal day PR 39.21% module temperature 39.5°C

Sunny day PR 25.94% module temperature 43.5°C

Figure 52 Photovoltaic system of SIECT

Source: Seung-Ho Yooa and Eun-Tack Lee [48]

Overall, BIPV installed on a building façade with the proper tilt angle causes more electrical energy production than vertical slope installation. The temperature of the module was less because of the better ventilation. In contrast, the performance was reduced if the installation was at a lower level because of buildings shade covering the modules.

5.2 The optimization of shading type research

5.2.1 Tilt of shading type in Hong Kong in reducing energy consumption

L.L. Sun and H.X. Yang [44] found that the impact of the tilt angles on the energy performance of the shading-type BIPV claddings is analyzed by calculation method in terms of annual electricity generation and annual cooling load reduction for a building. The study, as seen in the Figure 53, showed the annual energy generation was at the highest level at the slope angle of 20° while the local latitude of Hong Kong is around 22.3°N. Combining electricity generation and cooling load reduction, it can be concluded that the optimum tilt angles for the first type of shading-type BIPV claddings vary from 30 degrees to 50 degrees, while the optimum tilt angle for the second type is 0 degrees.

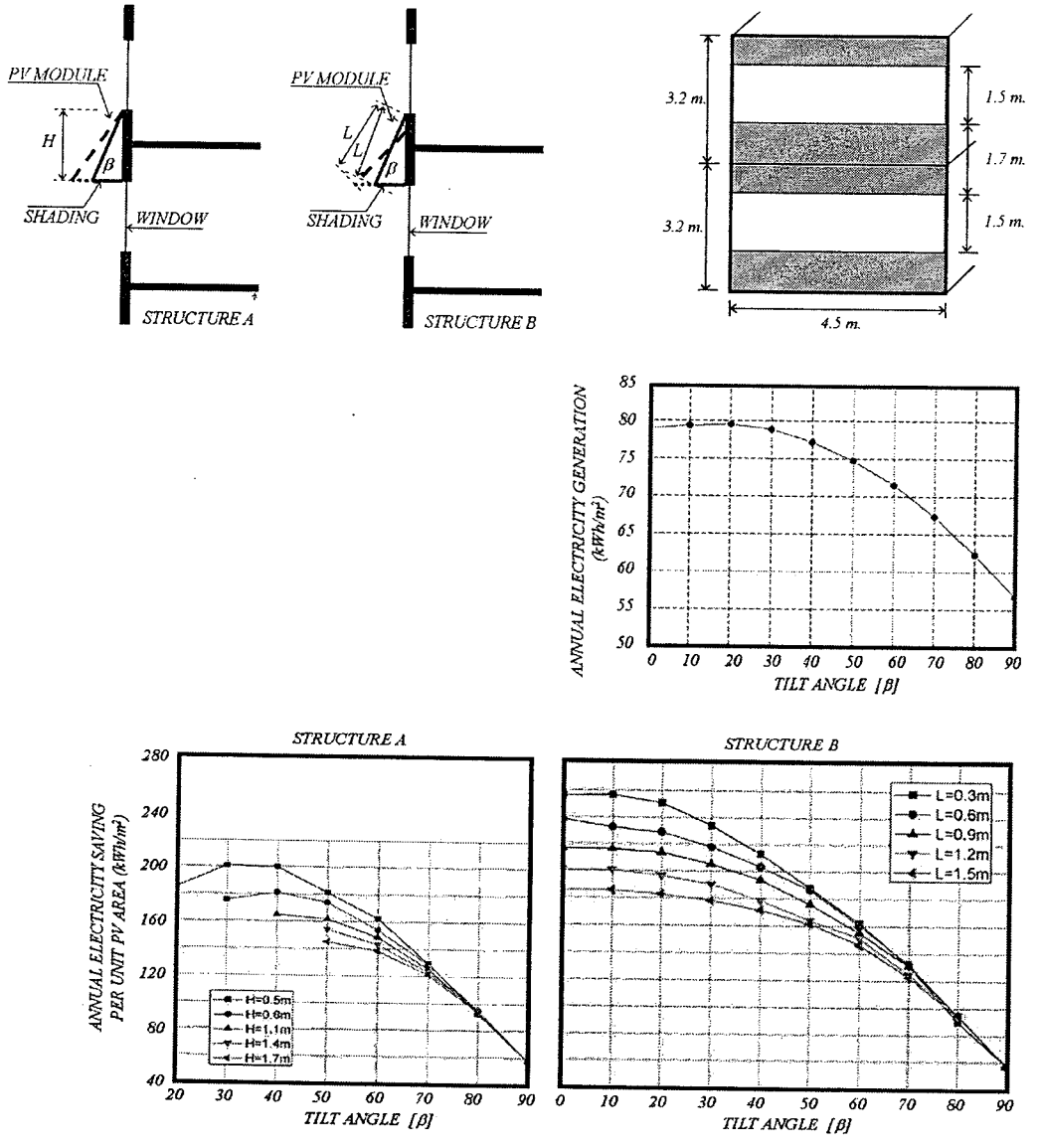

Figure 53 The study of L.L. Sun and H.X. Yang

Source: L.L. Sun and H.X. Yang [44]

5.2.2 Tilt of shading type in Taiwan

C.L. Chenga, C.Y. Chanb and C.L. Chen [7] found that the impact of the tilt angles on the energy performance of the shading-type was analyzed by regression method in a form of ratio of irradiance from slope surface to irradiance from flat surface from six locations in Taiwan. The results are shown in Figure 53, stating that the best tilt angle was between 0-30 degrees while the range of the location latitude was between 22-25 degrees.

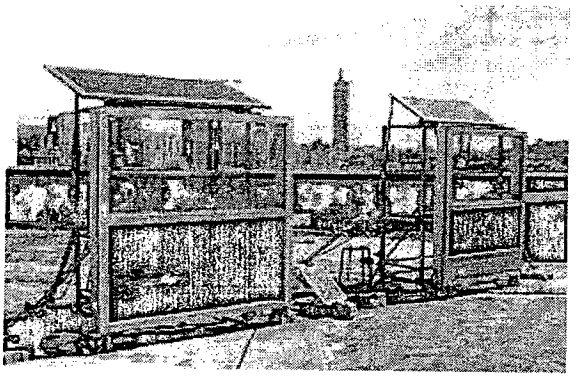

PV MODULEINTEGRATED IN WALL AND SHADING

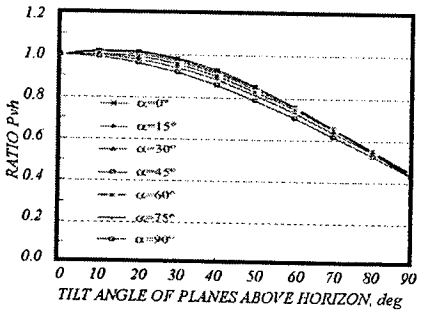

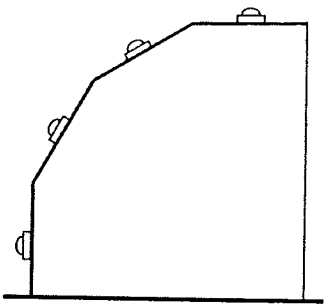

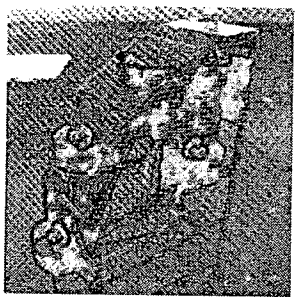

PYRANORMETERS INSTALLATION ON TILTED PLANES

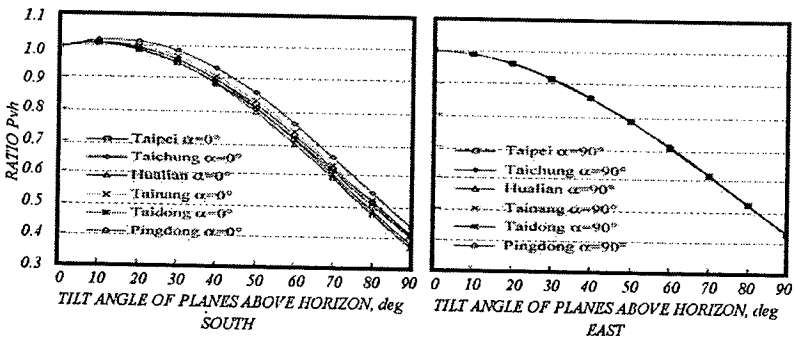

Figure 54 The study of C.L. Chenga, C.Y. Chanb and C.L. Chen

Source: Chao-Yu Chan [7]

5.2.3 E. Chanipat [55] found that the impact of the tilt angles on the energy performance of the shading-type was analyzed by computer simulation method, in the form of ratio of irradiance from slope surface to irradiance from flat surface in Bangkok, 14° latitude, on the southeast and the south as shown in Figure 54 stating that the best tilt angles were at 7 degrees and 12 degrees, respectively.

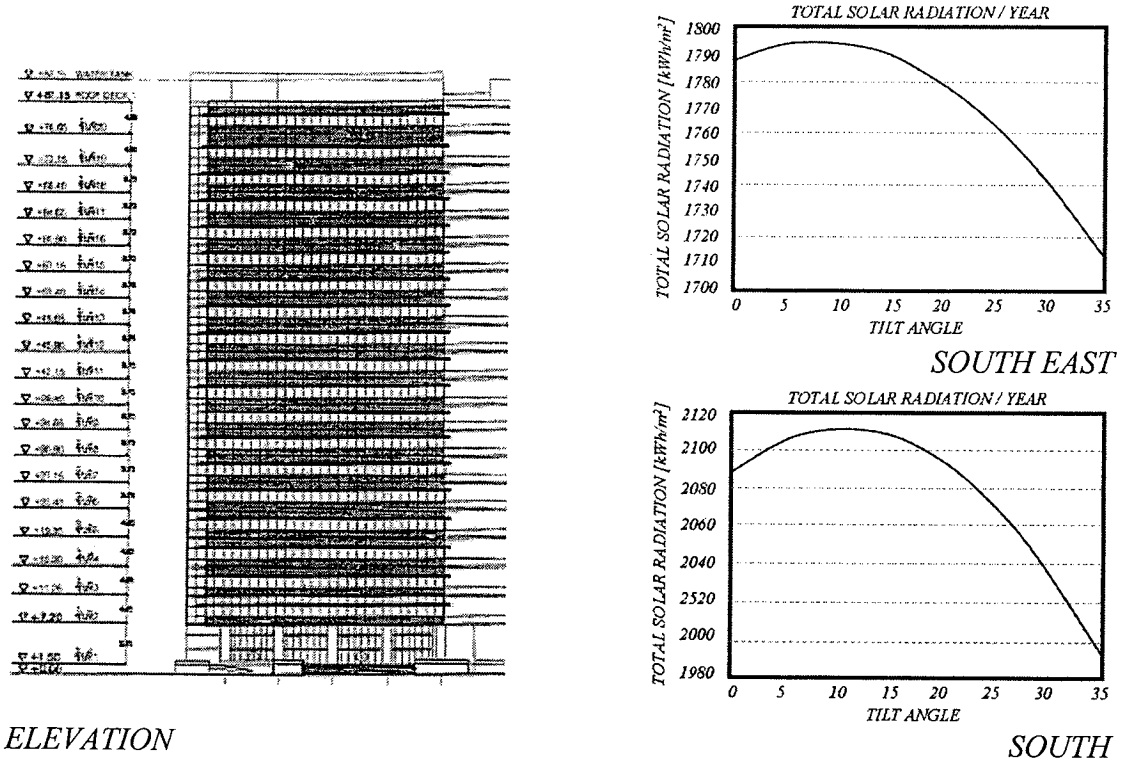

Figure 55 The study of E. Chanipat

Source: Euvananont, Chanipat [55]

5.2.4 S. Wanchart [56] found that the impact of the tilt angles on the energy performance of the louver type was analyzed by using comparison in the form of room temperature, internal illumination and power output of the PV generator in Bangkok, 13.5° latitude, on the south as shown in Figure 56 stating that the best tilt angles were at 7 degrees 22°.

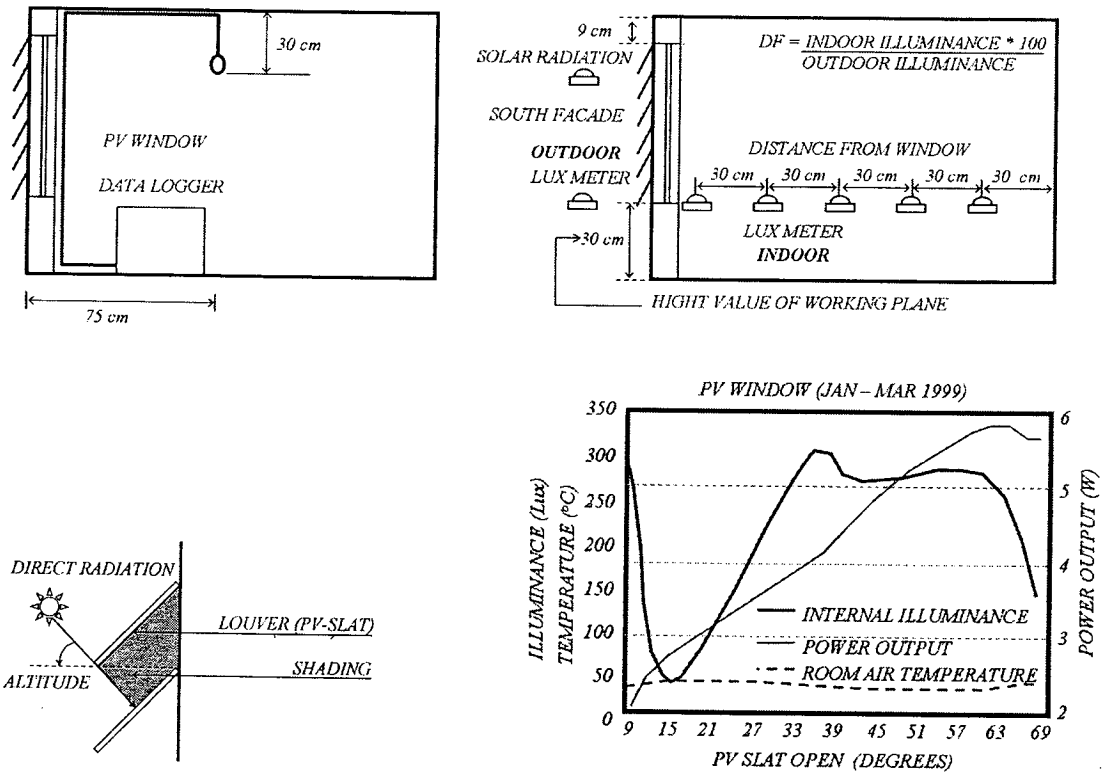

Figure 56 The study of S. Wanchart

Source: Supheng, Wanchart [56]

Conclusions of study showed the result of shading slope, according to the rule of thumb, depends on the latitude of each buildings location. Installation of different shading devices caused different results. The installation of a louver caused shade on the solar module due to the vertical overlapping.

The result parameter to design
1) The direction of PV module cause of the sun path.
2) The shading slope cause of latitude and building obstruction.
3) The half sky effect cause of building obstruction.
4) The shad of upper shading cause of shading obstruction.

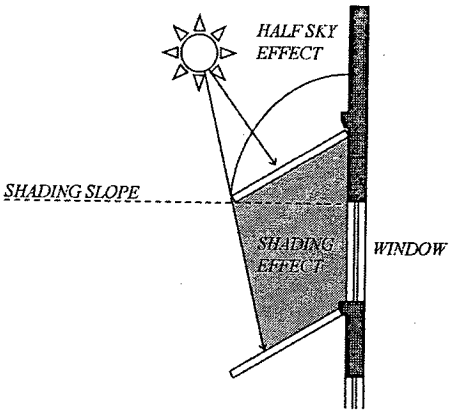

Figure 57 Summary of case studies

Cooling load

Solar heat gain from the solar radiation is protected by the shading device that is integrated with the photovoltaic system. Cooling shown in Figure 58 resulted from heat transfer in the forms of heat conduction, convection and radiation from air conditioning system by using electricity.

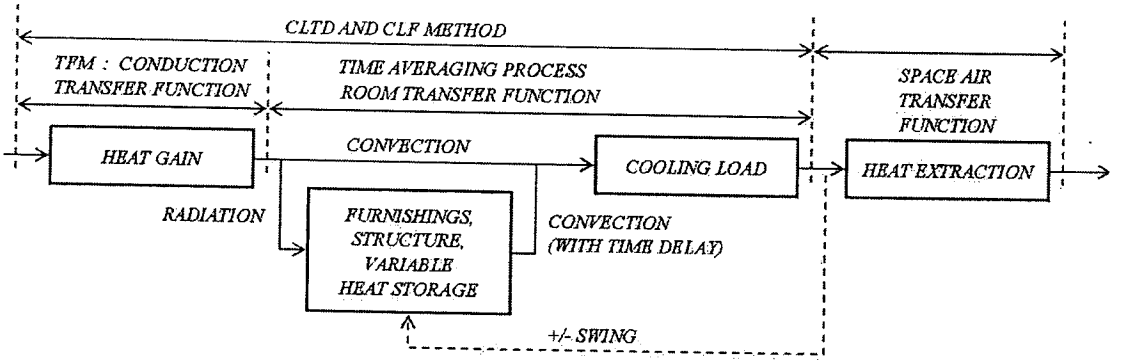

Figure 58 The procedure for calculating cooling load

Source: American Society of Heating, Refrigerating and Air-Conditioning Engineers [1]

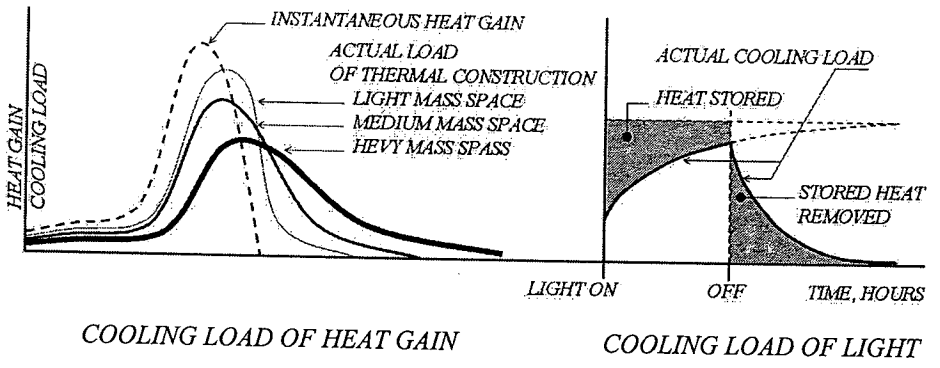

Figure 59 Heat delay of thermal construction and light

Source: American Society of Heating, Refrigerating and Air-Conditioning Engineers [1]

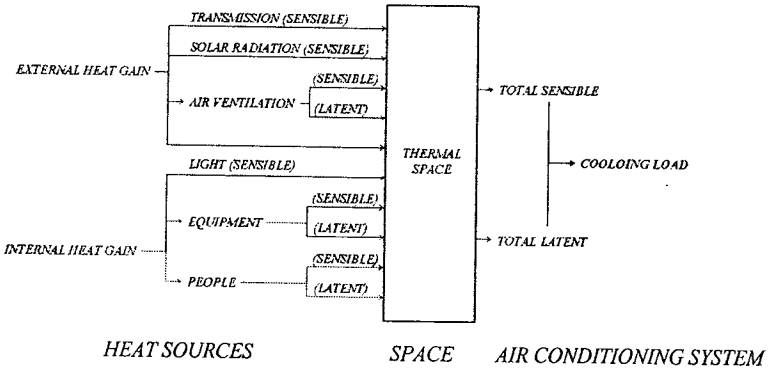

Figure 60 Cooling load calculations of sensible and latent heat

ASHREA [1] presented the CLTD and CLF methods used to estimate cooling coil load, as shown in Figure 58, which serves one or more conditioned space. CLTD method or Cooling Load Temperature Differential and CLF or Cooling Load Factors are steps in calculating cooling load from heat transferring through building envelop from both opaque and transparent parts and from internal heat load, as shown in Figure 60. This method includes the effect of time delay caused by thermal storage of materials, as shown in Figure 59. However, the scope of this research is only in the matter of fenestration and light sources, as shown in Figure 61.

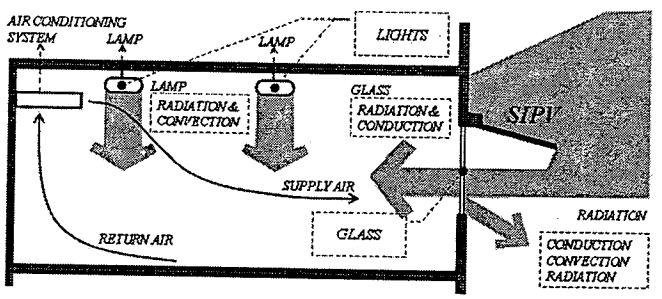

Figure 61 The components of heat load

The conditions of SIPV performance appraisal in cooling load is divided into 2 parts: cooling load because of glass and because of light bulbs.

1. Glass affects SIPV performance because heat is a part of the solar radiation that goes through the glass into the cooled space via conduction and radiation. It varies according to the properties of the glass and shading effect. It is calculated using equation as follows:

$$q_{cond} = (A)(U)(CLTD) \quad \text{Eq. 50}$$

$$q_{rad} = (A)(SHGF)(CLF)(SC) \quad \text{Eq. 51}$$

$$SC = SHGC(SC) \quad \text{Eq. 52}$$

$$U = 1/R_T \quad \text{Eq. 53}$$

$$R_T = R_o + dx_1/k_1 + dx_2/k_2 + dx_3/k_3 + \ldots + dx_n/k_n + R_{gap} + R_i \quad \text{Eq. 54}$$

CLTD, parameters are changed by outside and inside air temperature, which is calculated for an inside temperature of 25.5°C and outdoor maximum temperature of 35°C with an outdoor daily range of 12°C. Table 7 remains approximately correct for the other outdoor maximums of 34°C to 39°C and other outdoor daily ranges from 9°C to +19°C, provided the outdoor daily average temperature remains approximately 29.4°C. If the room air temperature is different from 25.5°C and/or the average daily outdoor temperature is different from 29.4°C, the following rules apply:

1.1 For room air temperature less than 25.5°C, subtract the difference.

1.2 For average daily outdoor temperature less than 29.4°C, subtract the difference between 29.4°C and the daily average temperature; if greater than 29.4°, add the difference.

Table 7 Cooling Load Temperature Differences (CLTD) of clear glass

Solar time	(h)	1	2	3	4	5	6	7	8	9	10	11	12
CLTD	(°C)	1	0	-1	-1	-1	-1	-1	0	1	2	4	5
Solar time	(h)	13	14	15	16	17	18	19	20	21	22	23	24
CLTD	(°C)	7	7	8	8	7	7	6	4	3	2	2	1

Source: American Society of Heating, Refrigerating and Air-Conditioning Engineers [1]

SHGF, the maximum Solar Heat Gain Factor, varied by orientation, latitude and month, as shown by the comparison in Table 8. The maximum solar heat gain factor for externally shaded glass (based on a ground reflectance of 0.2) is shown in Table 9.

Table 8 Maximum Solar Heat Gain Factor, W/m^2, for 14°N latitude of glass

	Orientation					
month	**N**	**NE/NW**	**E/W**	**SE/SW**	**S**	**H**
Jan	96.5	186.5	674.0	785.5	601.0	804.5
Feb	105.5	317.0	735.0	724.0	453.0	885.0
Mar	112.0	454.0	751.0	610.5	261.5	927.5
Apr	124.5	552.5	716.0	460.5	134.0	913.5
May	176.5	604.0	673.5	348.5	127.5	886.5
Jun	222.5	618.5	648.5	298.0	127.5	869.0
Jul	186.5	596.5	658.0	336.0	131.0	871.0
Aug	131.0	539.5	689.5	438.5	296.5	890.0
Sep	115.5	435.5	719.0	588.5	261.5	897.5
Oct	105.5	312.5	710.0	700.5	441.5	867.5
Nov	98.0	186.5	662.5	773.0	591.5	798.0
Dec	93.0	138.5	639.0	796.5	645.5	763.5

Source: American Society of Heating, Refrigerating and Air-Conditioning Engineers [1]

Table 9 Maximum Solar Heat Gain Factor, W/m^2, externally shaded

	Orientation					
month	**N**	**NE/NW**	**E/W**	**SE/SW**	**S**	**HOR**
Jan	98	98	107	117	120	50
Feb	107	107	114	120	123	50
Mar	114	117	123	126	123	60
Apr	126	130	133	129	126	76
May	137	142	142	129	126	88
Jun	142	148	145	129	126	98
Jul	142	145	148	133	129	98
Aug	133	136	145	136	133	88
Sep	117	120	129	133	129	73
Oct	107	107	120	126	126	60
Nov	101	101	107	120	123	54
Dec	95	95	101	114	117	47

Source: American Society of Heating, Refrigerating and Air-Conditioning Engineers [1]

Table 10 The Cooling Load Factor for glass without interior shading

Solar time	Orientation								
h	N	NE	E	SE	S	SW	W	SW	HOR
1	0.23	0.07	0.07	0.09	0.12	0.15	0.15	0.14	0.16
2	0.2	0.06	0.06	0.08	0.11	0.14	0.13	0.12	0.14
3	0.18	0.06	0.06	0.07	0.09	0.12	0.11	0.11	0.12
4	0.16	0.05	0.05	0.06	0.08	0.1	0.1	0.09	0.11
5	0.14	0.04	0.05	0.05	0.07	0.09	0.09	0.08	0.09
6	0.34	0.21	0.18	0.14	0.08	0.09	0.09	0.09	0.11
7	0.41	0.36	0.33	0.26	0.11	0.1	0.09	0.1	0.16
8	0.46	0.44	0.44	0.38	0.14	0.12	0.1	0.11	0.24
9	0.53	0.45	0.5	0.48	0.21	0.13	0.11	0.13	0.33
10	0.59	0.4	0.51	0.54	0.31	0.15	0.12	0.14	0.43
11	0.65	0.36	0.46	0.56	0.42	0.17	0.13	0.16	0.52
12	0.7	0.33	0.39	0.51	0.52	0.23	0.14	0.17	0.59
13	0.73	0.31	0.35	0.45	0.57	0.33	0.19	0.18	0.64
14	0.75	0.3	0.31	0.4	0.58	0.44	0.29	0.21	0.67
15	0.76	0.28	0.29	0.36	0.53	0.53	0.4	0.3	0.66
16	0.74	0.26	0.26	0.33	0.47	0.58	0.5	0.42	0.62
17	0.75	0.23	0.23	0.29	0.41	0.59	0.56	0.51	0.56
18	0.79	0.21	0.21	0.25	0.36	0.53	0.55	0.54	0.47
19	0.61	0.17	0.17	0.21	0.29	0.41	0.41	0.39	0.38
20	0.5	0.15	0.15	0.18	0.25	0.33	0.33	0.32	0.32
21	0.42	0.13	0.13	0.16	0.21	0.28	0.27	0.26	0.28
22	0.36	0.11	0.11	0.14	0.18	0.24	0.23	0.22	0.24
23	0.31	0.09	0.1	0.12	0.16	0.21	0.2	0.19	0.21
24	0.27	0.08	0.08	0.1	0.14	0.18	0.17	0.16	0.18

Source: American Society of Heating, Refrigerating and Air-Conditioning Engineers [1]

CLF, the Cooling Load Factor, varies by orientation, mass of construction, and effect interior shaded, which is shown in Table 9 to Table 11 for general cases of medium construction (100-mm concrete exterior wall, 100-mm concrete floor slab). It was estimated as mass per unit of floor area at 340 kg/m2.

SHGC, the Solar Heat Gain Coefficient, varies by the properties of glass and the incident angle. It was shown in Table 11.

R, Resistance value, varies by the properties of glass and air film both inside and outside of the glass, as shown in Table 12.

Table 11 The Solar Heat Gain Coefficient of glass

		SHGC						
		Center of glazing properties : Incidence angles						
	VT	Normal, 0	40	50	60	70	80	Hemisphere Diffuse
clear glass	0.90	0.86	0.84	0.82	0.78	0.67	0.42	0.78

Source: American Society of Heating, Refrigerating and Air-Conditioning Engineers [1]

Table 12 The resistance value of air

	Resistance value of air						
The property of glass surface	Air gap mm.						
	inside	5	6	7	10	13	outside
High radiation emission	0.120	0.084	0.091	0.097	0.110	0.119	0.044
Low radiation emission	0.299	0.167	0.196	0.208	0.278	0.345	-

Source: American Society of Heating, Refrigerating and Air-Conditioning Engineers [1]

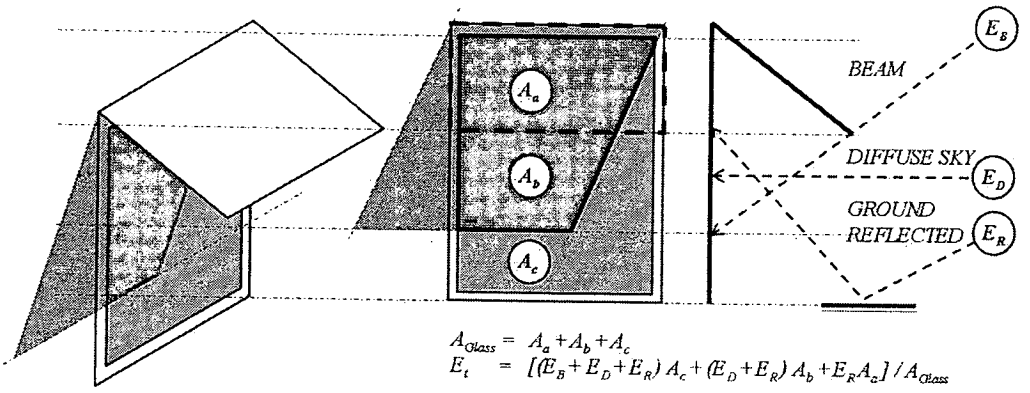

Figure 62 The shading area on the glass under shading device

SC, the Shading Coefficient, varies by the effect of effective shading in reducing the beam and diffuse radiation on the glass as shown in Figure 62. It calculated following Eq. 55.

$$SC = E_{twS} / E_{tw} \qquad \textit{Eq. 55}$$

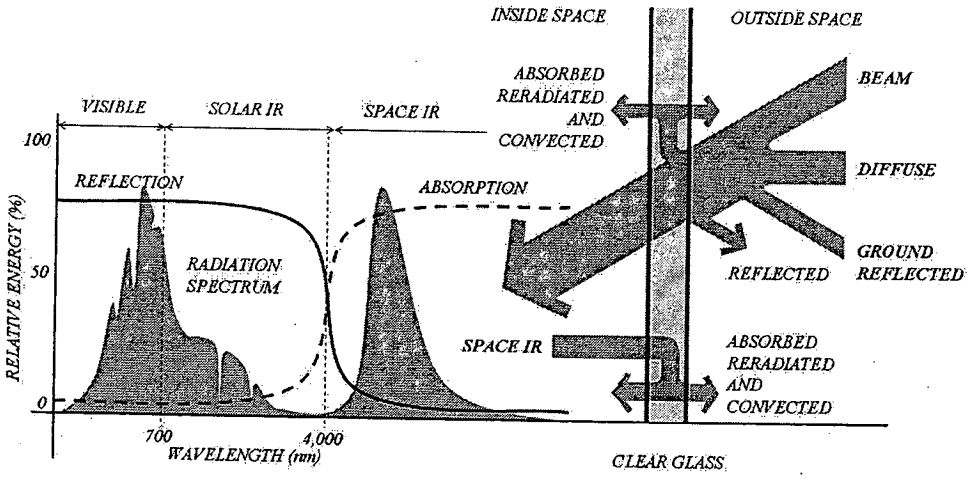

Figure 63 The heat transfer of the solar ray

Source: Lechner, Norbert [20]

2. Lights also affect SIPV performance. The internal cooling load varies by the light fixture type, supply and return ventilation, space furnishing and thermal structure. It can be calculated as follows:

$$q_{el} = (H\,G_{el})(CLF_{el}) \qquad Eq.\ 56$$

$$H\,G_{el} = (W_l)(F_{ul})(F_{sa}) \qquad Eq.\ 57$$

CLF_{el}, the Cooling Load Factor of the light, should be considered 1.0 when the cooling system operates only during the occupied hours; but if not under this condition, it should be considered as shown in Table 13 to 15 in the case of lights being on for 8 hours.

Table 13 "a" coefficient

"a"	Furnishings	Air supply and return	Type of light fixture
0.45	Heavyweight, simple furnishings, no carpet	Low rate; supply and return below ceiling (V <= 2.5)	Recessed, not vented
0.55	Ordinary furniture, no carpet	Medium to high ventilation rate; supply and return below ceiling or through ceiling grill and space (V >= 2.5)	Recessed, not vented
0.65	Ordinary furniture, with or without carpet	Medium to high ventilation rate or fan coil or induction type air-conditioning terminal unit; supply through ceiling or wall diffuser; return around light fixtures and through ceiling space (V <= 2.5)	Vented
0.75 or greater	Any type of furniture	Ducted returns through light fixtures	Vented or free-hanging in air stream with ducted returns

Note: V is the room air supply rate in liters per second per square meter of floor area

Table 14 "b" classification

Room envelope construction1 (mass of floor area, kg/m^2)	Room air circulation and type of supply and return^2			
	Low	Medium	High	Very high
50 mm wood floor (50)	B	A	A	A
75-mm concrete floor (200)	B	B	B	A
150-mm concrete floor (370)	C	C	C	B
200-mm concrete floor (590)	D	D	C	C

Note: 1. Floor covered with carpet and rubber pad; for a floor covered only with floor tile, take the next classification to the right in the same row.

2. These values are defined as follows:

2.1 *Low*: low ventilation rate -- minimum required to cope with cooling load from lights and occupants in interior zone. Supply through floor, wall, or ceiling diffuser. Ceiling space not vented and h = 2.3 W/m^2 °C, where h = inside surface convection coefficient used in calculation of b.

2.2 *Medium*: Medium ventilation rate, supply through floor, wall, or ceiling diffuser. Ceiling space not vented and h = 3.4 W/m^2 °C

2.3 *High*: Room air circulation induced by primary air of induction unit or by fan coil unit. Return through ceiling space and h = 4.5 W/m^2 °C

2.4 *Very high*: High room air circulation used to minimize temperature gradients in a room. Return through ceiling space and h = 6.8 W/m^2 °C

Table 15 Cooling Load Factor when lights are on for 8 hour

"a"	45				55				65				75			
"b"	A	B	C	D	A	B	C	D	A	B	C	D	A	B	C	D
h_{off}	Cooling Load Factor after lights are turned on															
1	0.02	0.07	0.11	0.14	0.01	0.06	0.09	0.11	0.01	0.04	0.07	0.09	0.01	0.03	0.05	0.06
2	0.46	0.51	0.55	0.58	0.56	0.6	0.63	0.66	0.66	0.69	0.72	0.73	0.76	0.78	0.80	0.81
3	0.57	0.56	0.58	0.60	0.65	0.64	0.66	0.67	0.73	0.72	0.73	0.74	0.80	0.80	0.81	0.82
4	0.65	0.61	0.60	0.61	0.72	0.68	0.68	0.68	0.78	0.75	0.75	0.75	0.84	0.82	0.82	0.82
5	0.72	0.65	0.63	0.62	0.77	0.71	0.70	0.69	0.82	0.77	0.76	0.76	0.87	0.84	0.83	0.83
6	0.77	0.68	0.65	0.63	0.82	0.74	0.71	0.70	0.86	0.80	0.78	0.77	0.90	0.85	0.84	0.83
7	0.82	0.71	0.67	0.64	0.85	0.76	0.73	0.71	0.88	0.82	0.79	0.77	0.92	0.87	0.85	0.84
8	0.85	0.74	0.69	0.65	0.88	0.79	0.75	0.72	0.91	0.84	0.8	0.78	0.93	0.88	0.86	0.84
9	0.88	0.77	0.71	0.66	0.90	0.81	0.76	0.72	0.93	0.85	0.82	0.79	0.95	0.89	0.87	0.85
10	0.46	0.34	0.28	0.22	0.37	0.28	0.23	0.18	0.29	0.22	0.18	0.14	0.21	0.15	0.13	0.10
11	0.40	0.30	0.30	0.20	0.30	0.30	0.20	0.20	0.20	0.20	0.20	0.10	0.20	0.10	0.10	0.10
12	0.30	0.28	0.25	0.21	0.24	0.23	0.20	0.17	0.19	0.18	0.16	0.13	0.13	0.13	0.11	0.10
13	0.24	0.25	0.23	0.20	0.19	0.20	0.19	0.17	0.15	0.16	0.15	0.13	0.11	0.11	0.10	0.09
14	0.19	0.22	0.22	0.20	0.16	0.18	0.18	0.16	0.12	0.14	0.14	0.13	0.09	0.10	0.10	0.09
15	0.15	0.20	0.20	0.19	0.13	0.16	0.17	0.16	0.10	0.13	0.13	0.12	0.07	0.09	0.09	0.09
16	0.12	0.18	0.19	0.19	0.10	0.15	0.16	0.15	0.08	0.12	0.12	0.12	0.06	0.08	0.09	0.08
17	0.10	0.16	0.18	0.18	0.08	0.13	0.15	0.15	0.06	0.10	0.11	0.11	0.05	0.07	0.08	0.08
18	0.08	0.15	0.17	0.18	0.07	0.12	0.14	0.14	0.05	0.09	0.11	0.11	0.04	0.07	0.08	0.08
19	0.06	0.13	0.16	0.17	0.05	0.11	0.13	0.14	0.04	0.08	0.10	0.11	0.03	0.06	0.07	0.08
20	0.05	0.12	0.15	0.16	0.04	0.10	0.12	0.13	0.03	0.08	0.10	0.10	0.02	0.05	0.07	0.07
21	0.04	0.11	0.14	0.16	0.03	0.09	0.11	0.13	0.03	0.07	0.09	0.10	0.02	0.05	0.06	0.07
22	0.03	0.10	0.13	0.16	0.03	0.08	0.11	0.13	0.02	0.06	0.08	0.10	0.02	0.04	0.06	0.07
23	0.03	0.09	0.12	0.15	0.02	0.07	0.10	0.12	0.02	0.06	0.08	0.10	0.01	0.04	0.06	0.07
24	0.02	0.08	0.12	0.15	0.02	0.06	0.10	0.12	0.01	0.05	0.07	0.09	0.01	0.04	0.05	0.07

Note: h_{off} is the number of hours after lights are turned on.

a is coefficient.

b is classification.

Lights bulbs diffusing heat and light radiation because of energy conversion showing the loss of fluorescent lamps affect the calculation of cooling load as shown in Figure 64.

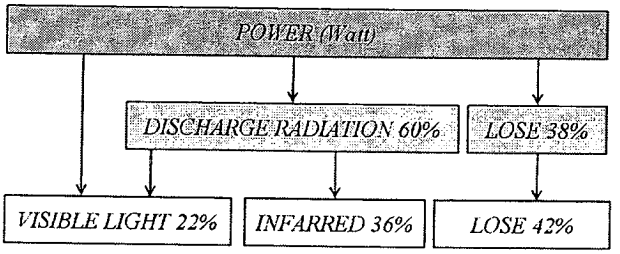

Figure 64 The heat conversion of a fluorescent lamp

Source: B. Sulee [3]

Daylight

1. Measurement light units

Daylight consists of UV, VIS and IR, which enters via the window and affects comfort in the living space in need for illuminance level and contrast for visualization. This can be measured in terms of light parameters, as shown in Figure 65 and Eq.58-60.

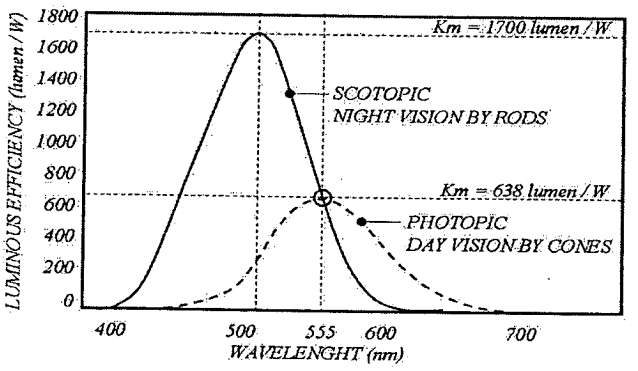

Figure 65 Human eye sensitivity and luminous efficiency

Source: Williamson, S. J. and Cummins, H. Z. [37]

$$F = 4\pi CP \qquad Eq.58$$

$$L = \rho E / \pi \qquad Eq.59$$

$$L = \tau E / \pi \qquad Eq.60$$

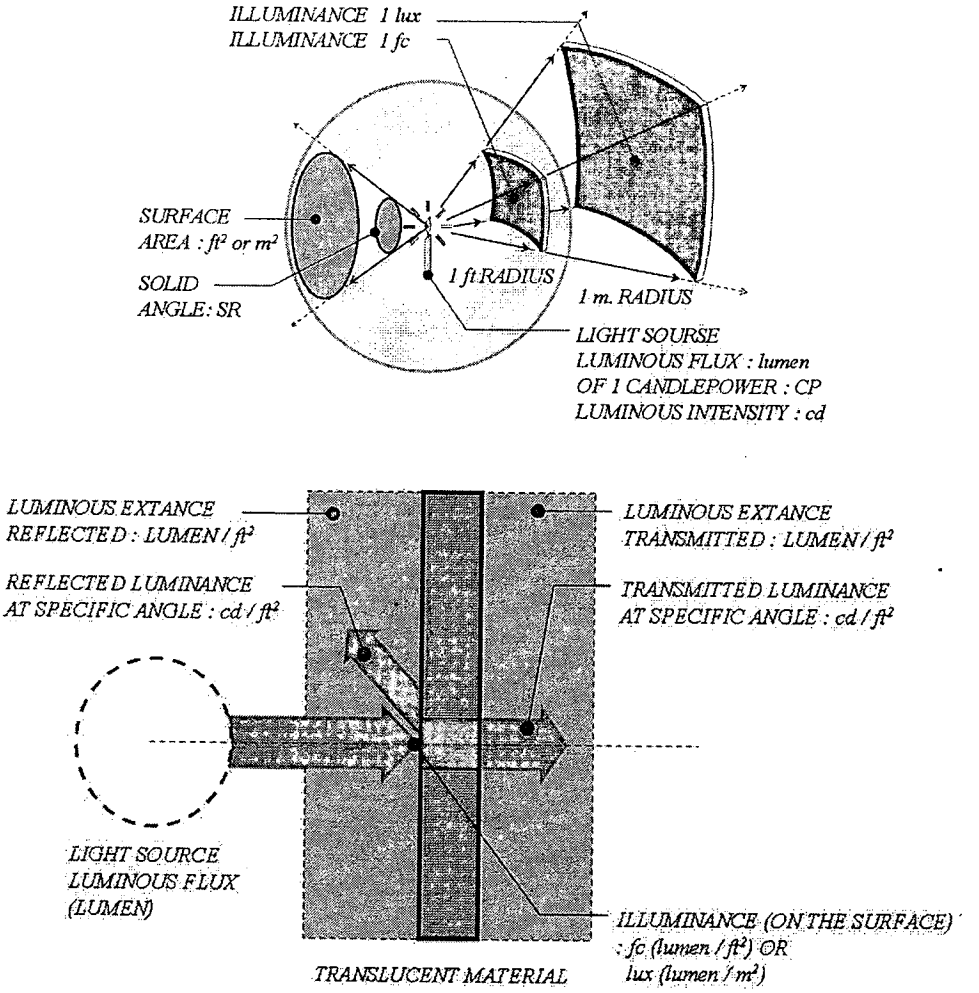

Figure 66 The measurement in term of light

Source: Egan, M. David [11]

2. Sky condition and sky model

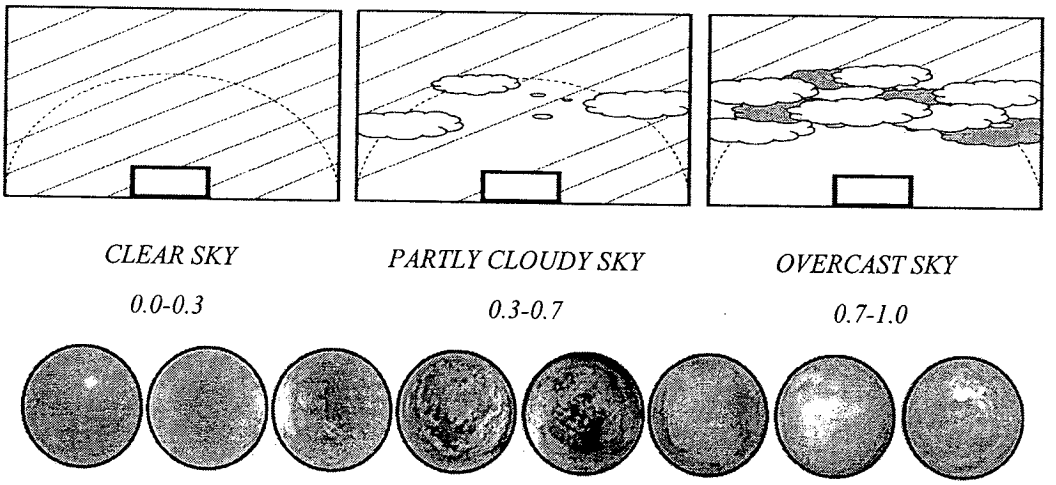

Figure 67 The sky condition

The sky conditions influencing the amount of daylight inside the building are separated into 3 forms: clear sky, partly cloudy sky and overcast sky. The differences are determined by cloud ratio, as shown in Figure 64, 65, 66 and Figure 67.

2.1 Uniform sky model

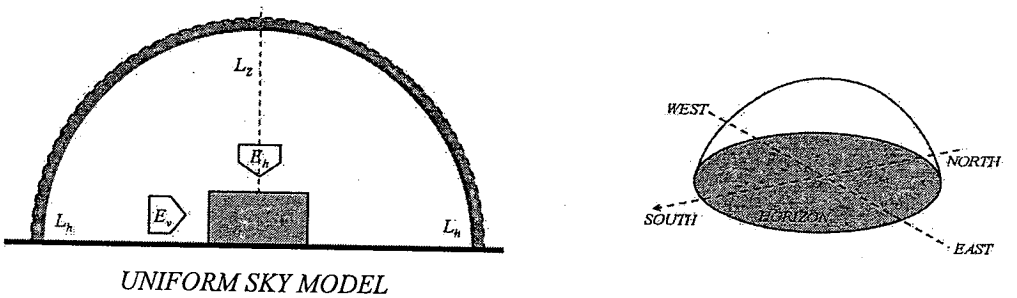

UNIFORM SKY MODEL

Figure 68 Uniform sky model

Source: Cowan, Henry, J. [9]

This module appears in constantly luminous daylight with a luminous value of 0.5 at the vertical view.

$$E = \pi L \quad Eq.61$$

$$E_h = \pi L \quad Eq.62$$

$$E_v = (1/2)\,\pi L \quad Eq.63$$

2.2 Overcast sky model

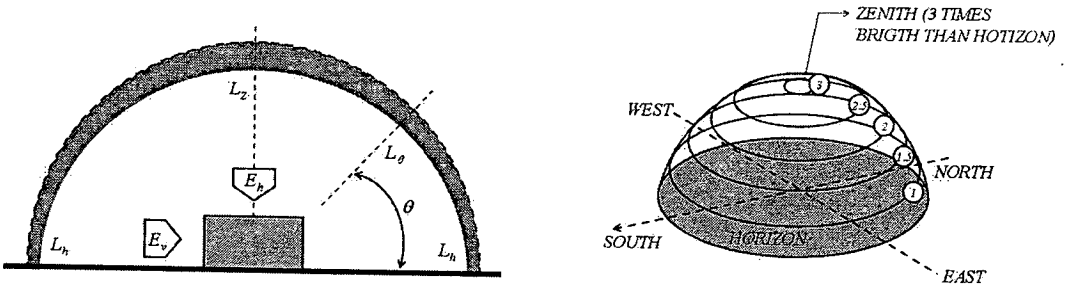

CIE OR OVERCAST SKY MODEL

Figure 69 Overcast sky model

Source: Cowan, Henry, J. [9]

$$L_\theta = (1/3)\,L_Z(1 + 2\sin\theta) \quad Eq.64$$

$$L_h = (1/3)\,L_Z \quad Eq.65$$

$$E_h = (7/9)\,\pi L_Z \quad Eq.66$$

$$E_v \approx L_Z \quad Eq.67$$

This module shows maximum luminosity at the horizontal plane, which will be decreased to 1/3 at the vertical view.

2.3 Clear sky model

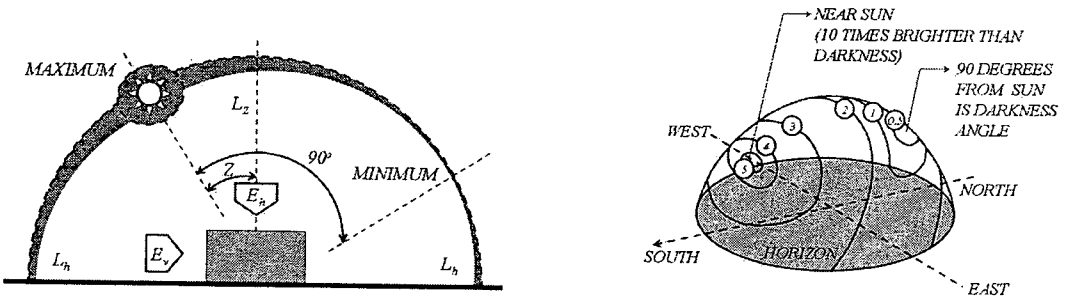

CLEAR SKY MODEL

Figure 70 Clear sky model

Source: Cowan, Henry, J. [9]

$$L_\theta = \frac{(1-e^{-0.32/\sin\theta})(0.91+10e^{-3a}+0.45\cos^2 a)\,L_Z}{0.274(0.91+10e^{-3Z}+0.45\cos^2 Z)} \qquad Eq.68$$

$$L_\theta = constant\ ;\ 15 < \theta < 90 \qquad Eq.69$$

$$= L_Z / \sin\theta \qquad Eq.70$$

$$= L_Z / \sin 15^o = 3.86\,L_Z \qquad Eq.71$$

This module shows maximum luminosity at the sun position and minimum luminosity at 90 degrees measured from the maximum point.

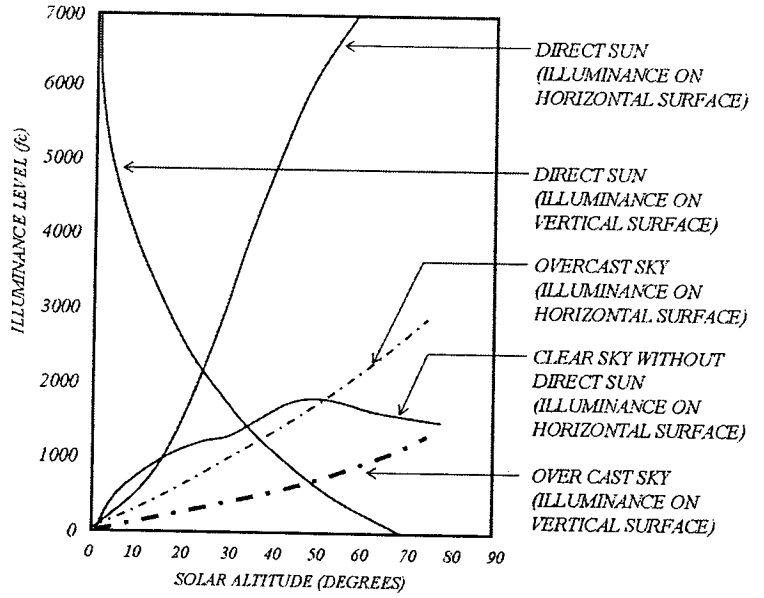

< *The vertical surface was received the illuminance around a half compare with the horizontal surface.*

Figure 71 The illuminance level comparison

Source: Egan, M. David [11]

Figure 71 explains natural light under weather conditions comparing illuminance due to the fact that location of solar attitude is related to direction of vision towards the daylight source or window.

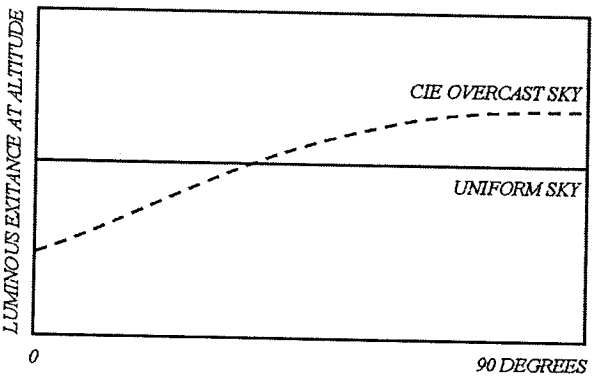

< *The Uniform sky has luminous constantly around the average of the overcast sky model.*

Figure 72 The comparison between uniform sky and overcast sky models

Source: Cowan, Henry, J. [9]

3. Efficacy of daylight

As shown in Figure 73, Daylight is a light source with high efficacy compared to artificial light sources, containing the approximate values of 120 lumen/Watt for average sky, 150 lumen/Watt for clear sky, and below 120 lumen/Watt for average sky with sun rays.

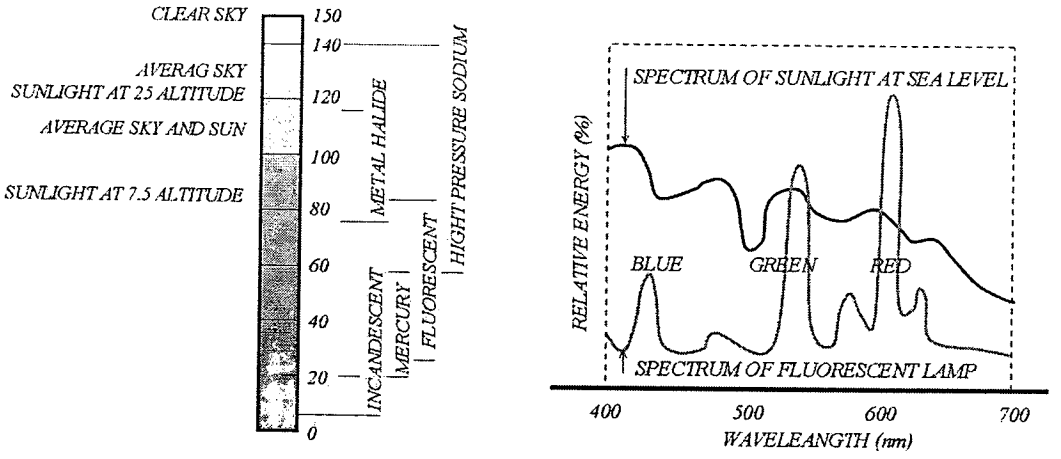

Figure 73 The efficacy of daylight and artificial light sources

Source: M. David Egan and Victor W. Olgyay [21]

4. Day lighting design

Daylight Factor, DF, is the method for prediction by math models described in Eq.72-73 for lumen method and Eq.74-76 for experimental method. In experimental study, a mirror box was used to collect data, as shown in Figure 75. A mirror box is a tool that reproduces an overcast sky. However, if the data collection was meant to come from the real sky, then a clear sky or overcast sky should be considered. As for a partly cloudy sky, it is easily changeable, unstable and difficult to study.

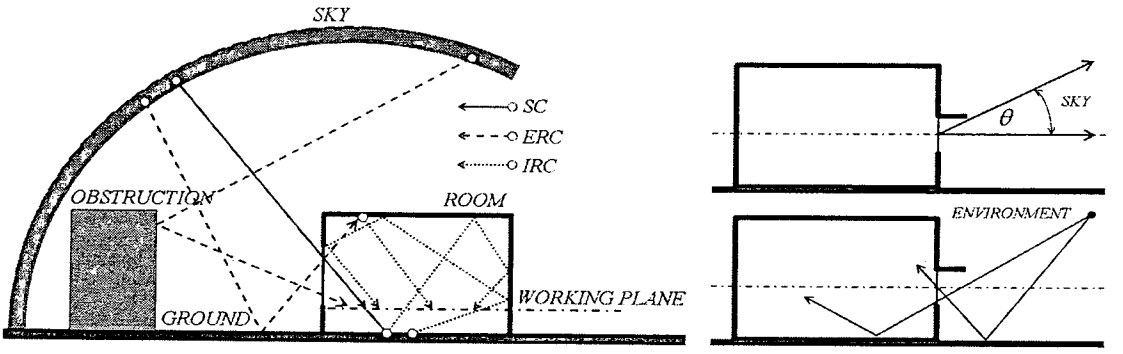

Figure 74 The daylight part into the room

Source: Cowan, Henry, J. [9]

$$DF_{av} = C\,A_W\,\tau\,MF\,(GBC) / A_t\,(1 - \rho_{av}) \qquad Eq.72$$

$$DF_{av} = A_t\,\tau\,MF\,(GBC)\,[\,(C/A_L)+(C\,\rho_L + 0.05\rho_U)/A_t\,(1 - \rho_{av})] \qquad Eq.73$$

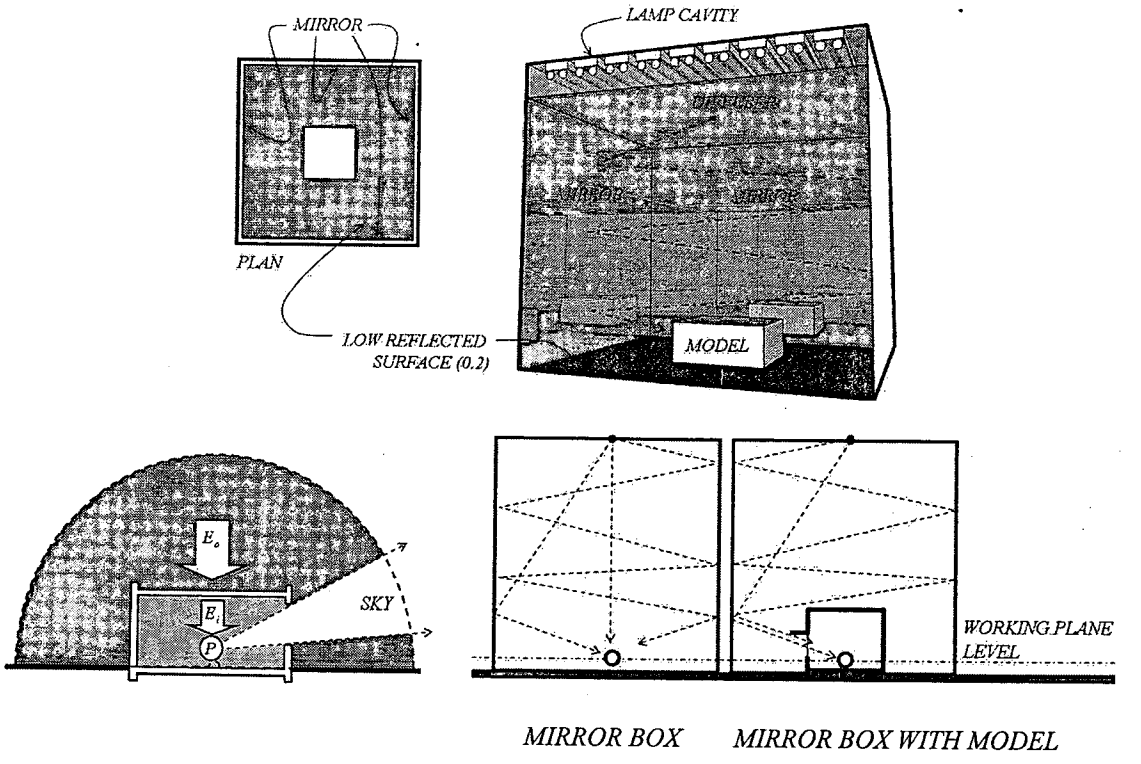

Figure 75 The mirror box explanation

Experimental methods including the mirror box or real sky used to evaluate daylight factor will apply physical model with enough scale to enter light sensors in each position on the working plane. However, in the case study under real sky conditions, the thing that should be watched out for is the shade of clouds blocking out the sun light and the amount of clouds in the sky. The data collection should be only for light from the sky, not direct solar radiation.

$$DF = E_i / E_o \qquad Eq.74$$

$$DF = SC + IRC + ERC \qquad Eq.75$$

$$E_i = DF(E_{sky}) \qquad Eq.76$$

5. Illumination on the working plane

Illuminance is light measured on the plane which, in this study, was the working plane at a height of 0.75 m varying according to need in usability. The suitability is shown in Table 2, 3, 4, 5, 6, 7, 8, 9, 10, 11, 12, 13, 14 and Table 15 compared using numbers of standards such as Thai building code, French CIE standards, American IES standards to DF suitable for each type of activity.

Table 16 The comparison of illumination standards

Working plane	Building code (Lux)	CIE (Lux)	EIS (Lux)	DF (%)
General area	300	150-200-300	200-300-500	5
Meeting	300	300-500-750	200-300-500	5
Office working	300	300-500-750	500-750-1,000	5
Walking area	200	50-100-150	50-75-100	2
Parking area	50	50-100-150	50-75-100	2

Note: CIE is The International Commission on Illumination (The Commission Internationale de I'Eclairage).
EIS is Illuminating Engineering Society of North America.

Source: Benjamin Stein and John S. Reynolds [4]; I, Kasadit [15]; Srisutapan, A and T. Panjira [29]

Lighting systems were designed to be proper for usability and the amount of electric power per unit of utility space according to type of building in need of energy saving. Details from building law for energy conservation are defined in Table 17. The aforementioned values resulted from design and determination of type of light bulb with reflector, type of ballast and light control such as on/off technique or dimming technique to create usability as long as needed, especially with daylight.

Table 17 The maximum power of lighting system defined by building code

Building type	Average power (W/m^2)
Education, Office	14
Shopping center, Rental shop, Theater	18
Hotel, Residential, Hospital	12

6. Daylight Glare Index

Glare is one of the qualitative indicators affecting usability in relation with angles as shown in Figure 76. In this research, windows are a light source causing glare when looking out the window which changes throughout the day, as shown in Figure 77 by the calculation of daylight glare index (DGI) using Eq.77-85. Glare is an important parameter affecting usability when gazing out a window. The discomforting glare occurs when the light source coming through the window is much brighter than requirement for sensation of the eyes. Disabling glare occurs when the light affects the ability to see. Conditions of differences of light in the form of contrast ratio were suitable at 3:1, which was the ratio of the viewing area to ambient area, 10:1 for the ratio of the viewing area to background area, and 50:1 for ratio of the highlighted object to the ambient area [21]. However, Hopkinson presented the GI, Glare Index, in 1960 and was supported by a field study in 1970 that expressed GI as Eq.77-85 [8]. Then it was modified from dGI to DGI as described by Eq.86.

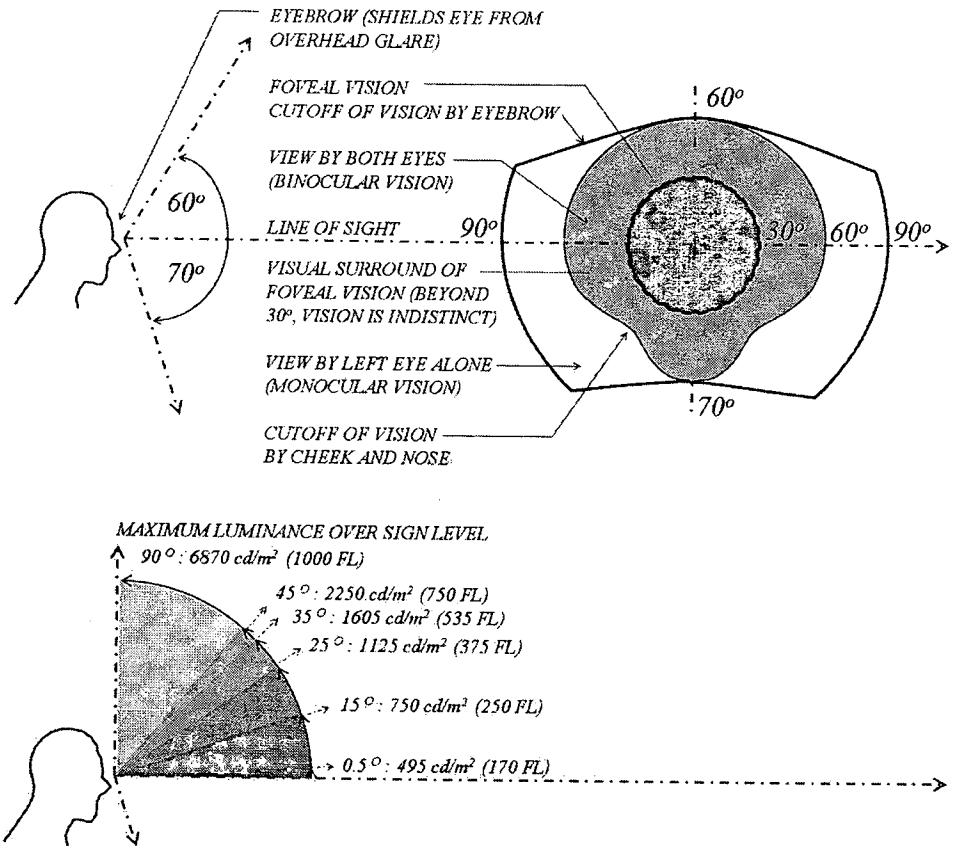

Figure 76 The eyes view and luminance sensation

Source: Claude L. Robbins [8]; Flynn, John E., Kremers, Jack A., Segil, Arthur W. and Staffy Gary R. [13]; M. David Egan and Victor W. Olgyay [21]

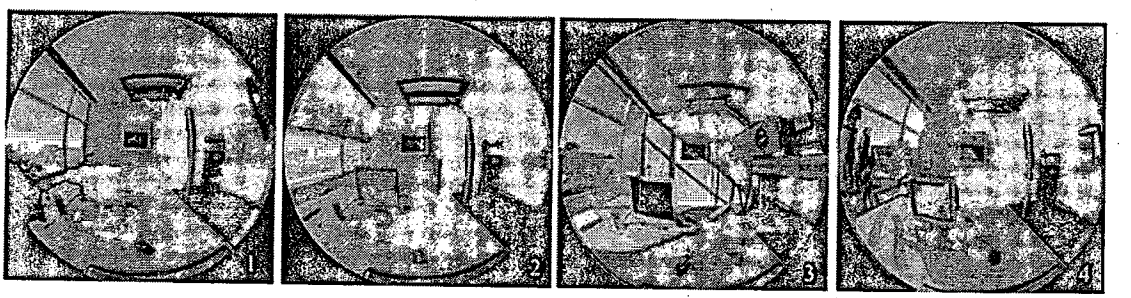

Figure 77 The glare effect from the side window

Source: Andersen, Marilyne [58]

Hopkinson model

$$dG = 11\{(L_s^{1.6})(\Omega^{0.8})/L_b+[(0.07(\omega^{0.5})(L_a)]\} \quad Eq.77$$

$$L_a = 0.3178\,E_a \quad Eq.78$$

$$L_s = (E_{sp}/V)(T_g/0.85) \quad Eq.79$$

$$L_b = [(IRE + ERE)/\pi](z)(T_g/0.85) \quad Eq.80$$

$$z = (1.9785\ln E_H) - 15.9164 \quad Eq.81$$

$$v = 0.8536\,e^{0.0733A} \quad Eq.82$$

$$L/d = w/d \quad Eq.83$$

$$L/d = l/d \quad Eq.84$$

$$dGI = 10\log_{10}\Sigma dG \quad Eq.85$$

Parameter A is the angle between the direction of view of the eyes and the center of the aperture.

Modified model

$$DGI = dGI - (x+y) \quad Eq.86$$

$$dGI = 12.02\,e^{(0.0309)(GI)} \quad ; for\ 10 < GI < 28 \quad Eq.87$$

$$x = (E_{dGI}^{-0.459})(100\,F_{dGI}^{3.148}) \quad Eq.88$$

$$F_{dGI} = D_{max}\{1+[E_{dGI}2 / E_{co}(E_{co} - 2E_{max})]\} \quad ; E_{dGI} < E_{co} \quad Eq.89$$

$$= [(2D_{max};)/(E_{co} - 2E_{max})](E_{dGI} - E_{max}) \quad ; E_{dGI} < E_{co} \quad Eq.90$$

$$y = (10\,x\,\rho_r) - 5 \quad ; 0.3 < \rho_r < 0.9 \quad Eq.91$$

Table 18 The Daylight Glare Index category

Illuminance category		DGI_{max}
General lighting throughout spaces		
Public spaces with dark suroundings	A	24
Simple orientation for short temporary visits	B	26
Working spaces where visual tasks are only occasionally performed	C	22

Source: Benjamin Stein and John S. Reynolds [4]; Claude L. Robbins [8]; Watson, Donald [36]

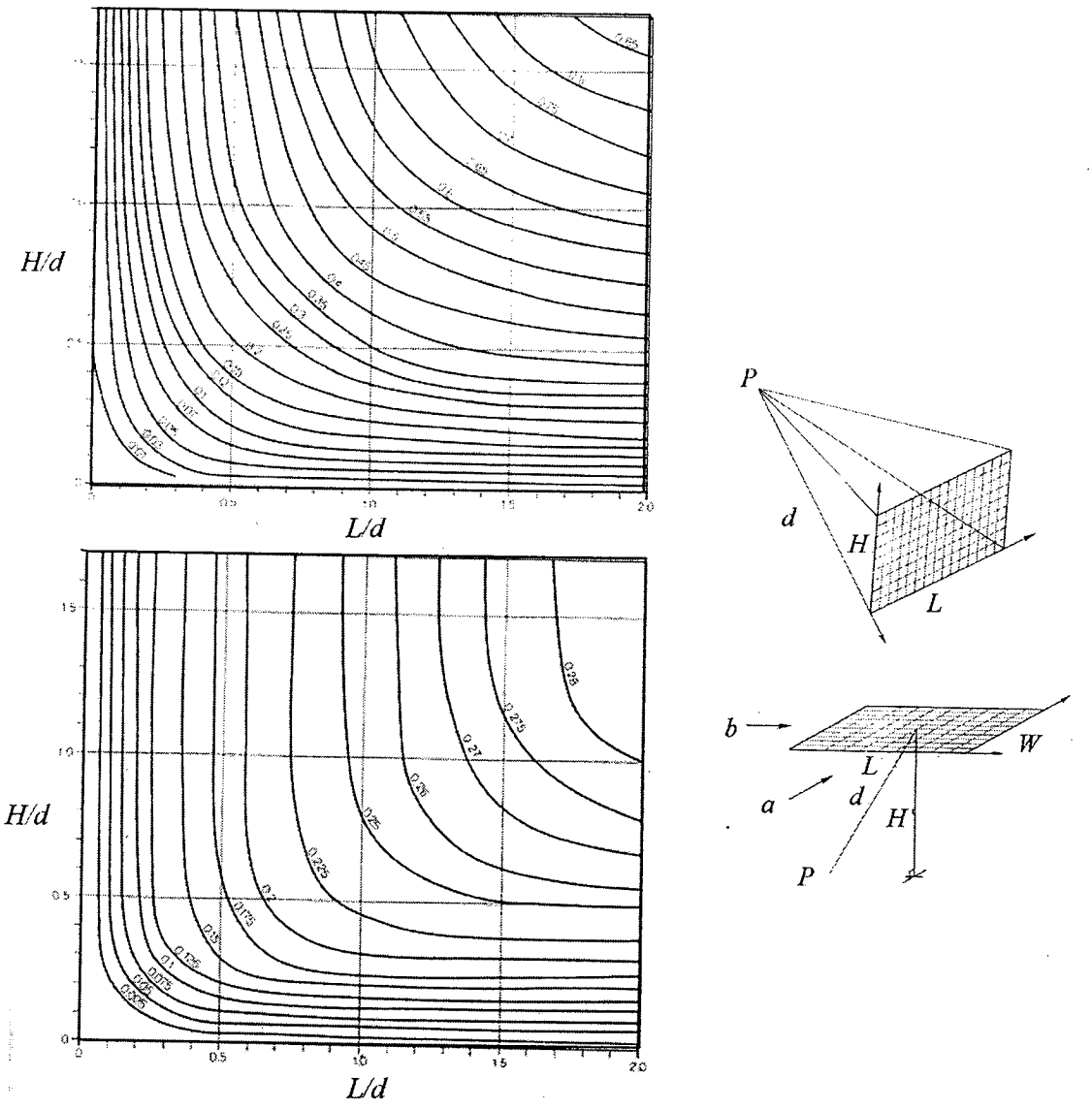

Figure 78 The eye parameters of Daylight Glare Index

Source: Claude L. Robbins [8]

Parameter D_{max} is the maximum fraction of the Standard Work Year (SWY) during which daylight can be used to replace or supplement electric light.

Table 19 Comparison between glare indexes (GI and DGI)

Degree of perceived glare	GI	DGI
Just perceptible	10.0	16
	13.0	18
Just acceptable	16.0	20
Borderline between comfort and discomfort	18.5	22
Just uncomfortable	22.0	24
	25.0	26
Just intolerable	28.0	28

Source: Claude L. Robbins [8]

7. Lighting design

The Lumen method is the light calculation method used to find sizes and arrangement of light bulbs. In uniform distribution design, the value estimation was a result from Eq.92-96 presented by IES standards [21].

$$F = (E)(A) / (CU)(LLD)(LDD) \quad Eq.92$$

$$CU = (5h_C)[(L + W) / (L \times W)] \quad Eq.93$$

$$CCR = (5h_{CC})[(L + W) / (L \times W)] \quad Eq.94$$

$$RCR = (5h_{RC})[(L + W) / (L \times W)] \quad Eq.95$$

$$FCR = (5h_{FC})[(L + W) / (L \times W)] \quad Eq.96$$

Light control is one of the strategies for saving lighting energy to be able to use energy as needed. It includes switches for on-off or dimming considering the amount of daylight, as shown in Figure 81 stating the results of using the strategies.

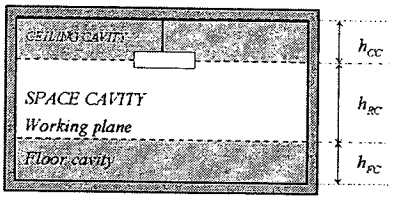

< *The separate cavity of the lighting effect.*

Figure 79 The spaces cavity of lighting

Source: M. David Egan and Victor W. Olgyay [21]

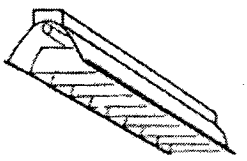

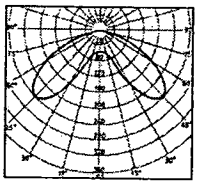

< *The efficiency of lighting need include the reflector what it concentrates the light though the working plane.*

Figure 80 The sample, Radial batwing, of light reflector distribution

Source: Benjamin Stein and John S. Reynolds [4]

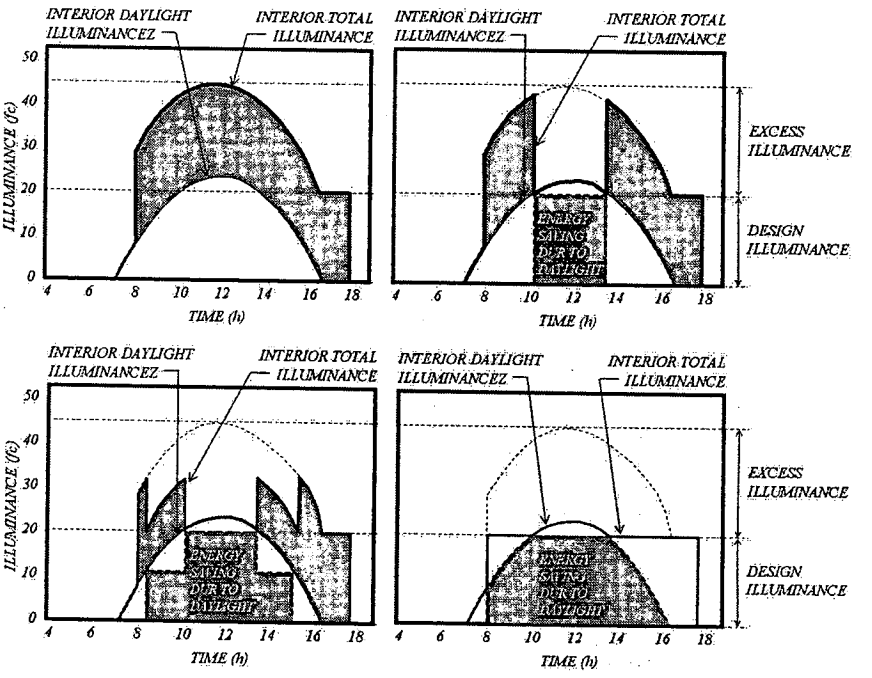

Figure 81 lighting control techniques

Source: Moor, Fuller [25]

Economic

1. Initial cost and life cycle cost

General PV systems are standalone system and grid connected system. The difference between the two mentioned systems is the battery element, which is easier to maintain and able to generate energy more reliably because it does not depending on an energy storage system leading to increasing system cost. When batteries and controller were excluded, its price ratio was about 23% of the system cost combined with saving labor for installation, structure, land used and building materials replaced with PV modules. This is the difference of the BIPV system.

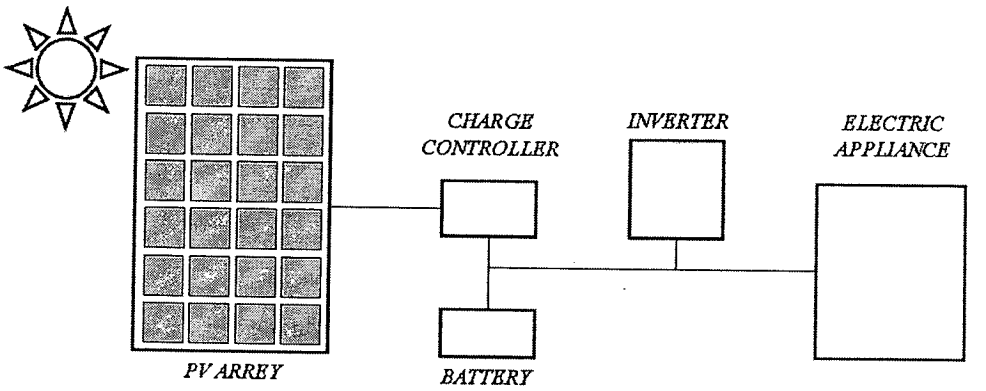

Figure 82 Stand alone PV system

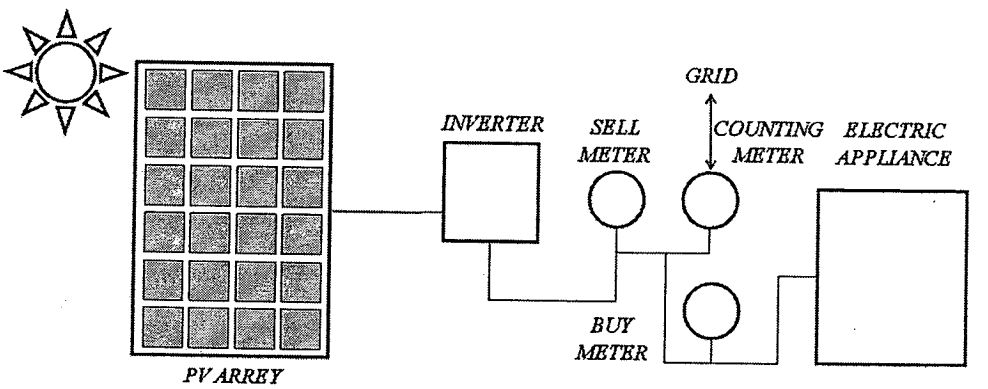

Figure 83 Grid connected PV system

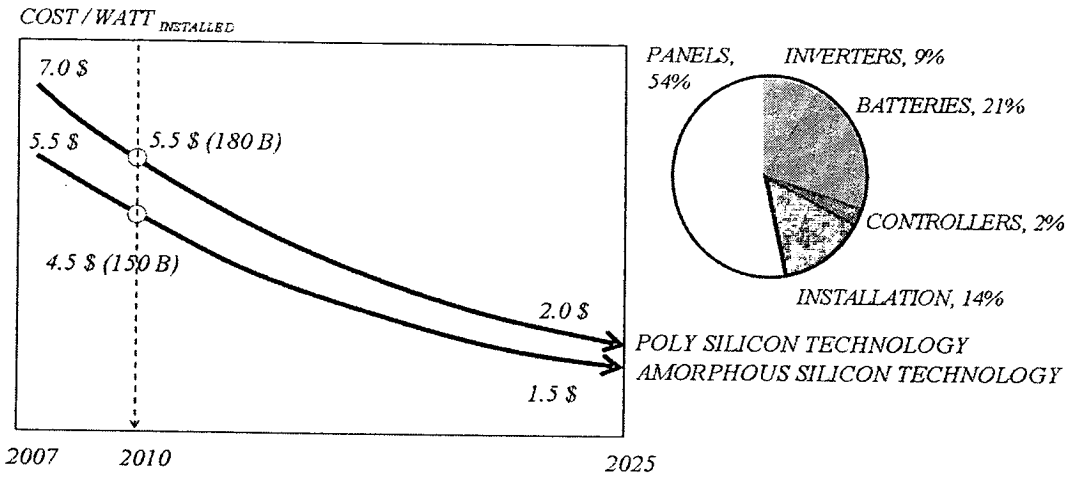

Figure 84 The trend of PV systems cost

Source: LaMonica, Martin [72]; Pearson, Chris [81]

The life cycle cost of a PV system is around 25 years guaranteeing only the PV modules integrated with the building envelope. Its life cycle operation is possibly more than 25 years including maintenance costs as a part of operation. Nevertheless, PV modules are expensive compared to general building materials as shown in Figure 85. The price could be lower when compared to some other types of decorative material. Besides, it is beneficial in clean energy generation concerning the environment. However, the cost of shading in the Thai market is estimated around \$30-\$60 per m^2.

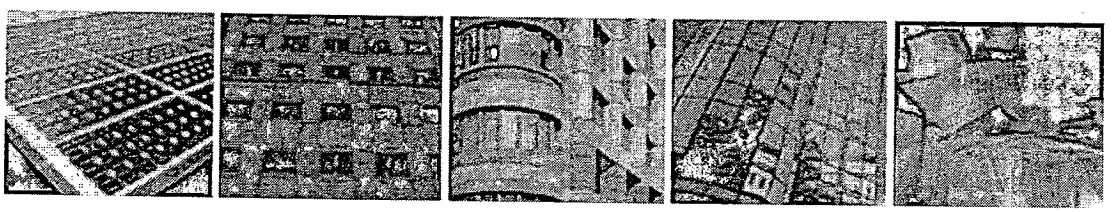

PV panel	Polished stone	Stone	Glass	Stainless steel
\$500-\$1500	\$2400-\$2800	\$800+	\$560-\$800	\$280-\$400

(These material costs were over investment for Thailand market in the present time.)

Figure 85 The comparison of material costs per square meter in 2002

Source: International Energy Agency [69]

2. Economical evaluation

The benefits of BIPV systems consist of 2 levels. First is the direct economic impact causing the decrease of construction material costs, electricity costs, enhancing power quality and reliability and providing tax credits. Second is the indirect economic impact due to environmental emissions reduction. For electrical costs, it is able to reduce energy used in air conditioning systems, save energy in lighting systems and produce energy used to replace energy from the grid. Therefore, to optimize investment, the costs and expected benefits must be acknowledged containing indicators as follows:

2.1 Payback period and break-event analysis

This method is used to predict the year that the benefits and costs will be equal. The break-even is used to compare the design solution for the final decision.

2.2 Benefits-Costs ratio (B/C)

This method converts to the present value of cost by using the present-worth method shown in Eq.98. Then, B/C and the results of comparison between benefits and costs leading to the investment decision are considered.

$$Payback = PVB / PVC \qquad Eq.97$$

$$P = F[1/(1+i)^t] \qquad Eq.98$$

$$PVB = \Sigma[B/(1+i)^t] \quad , \text{ during } t=1 \text{ to the last year} \qquad Eq.99$$

$$PVC = K + \Sigma[C/(1+i)^t] \quad , \text{ during } t=1 \text{ to the last year} \qquad Eq.100$$

$$B/C = PVB/PVC \qquad Eq.101$$

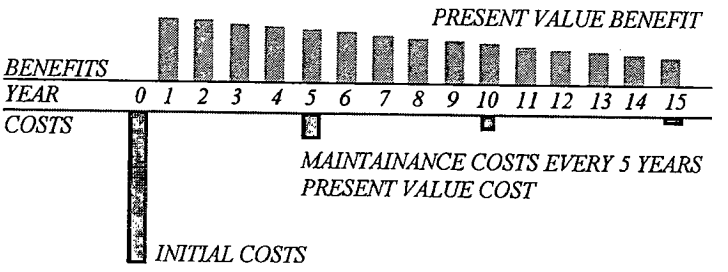

< *The decision to investment uses the cash flow that calculates from economical methods.*

Figure 86 An example of cash flow model

Summary of the review

From the study, it can be concluded and shown in Figure 87 to lead to design a studying process as below:

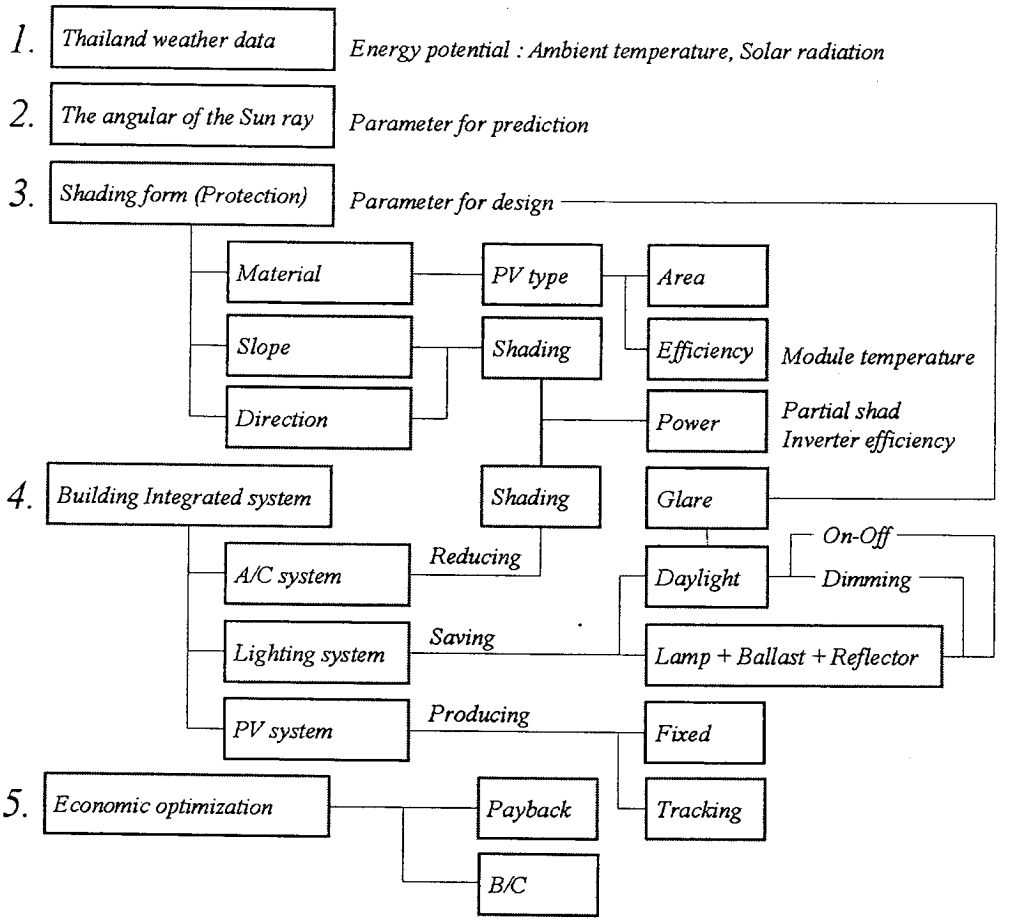

Figure 87 The summary review of the literature

1. Thailand has an solar energy potential average of about 5 kWh/m^2-Day, which is enough for investment.

2. Thailands latitude is between 6-20 degrees and longitude is between 97-101degrees, considering Bangkok, 14 degrees, as the center of Thailand.

3. Parameters affecting energy generated from PV systems include PV technology, slope and direction of PV module installation, which are needed to avoid the shade covering the area of the solar module.

4. The benefits of shading devices integrated with photovoltaic system include reduction of air conditioning system, electricity saving of lighting system and energy generation from the PV system.

5. Shading devices integrated with photovoltaic system can reduce cost of building and be more beneficial than general installation, which only generates energy. Therefore, it is more attractive for investment.